Lithospheric Fabric in Central North America: the Superior Province and the Mid-Continent Rift

by

Oyekunle Babatunde Ola

A Thesis submitted to the Faculty of Graduate Studies of

The University of Manitoba

in partial fulfilment of the requirements of the degree of

MASTER OF SCIENCE

Department of Geological Sciences

University of Manitoba

Winnipeg

THE UNIVERSITY OF MANITOBA

FACULY OF GRADUATE STUDIES

*****

COPYRIGHT PERMISSION PAGE

Lithospheric Fabric in Central North America: the Superior Province and the Mid-Continent Rift

by

Oyekunle B. Ola

A Thesis submitted to the Faculty of Graduate Studies of The University of Manitoba in partial fulfilment of the requirements of the degree of

Master of Science

Acknowledgements

I would never have been able to finish my thesis without the guidance of my committee members. My deepest gratitude goes to my admirable supervisor, Dr. Andrew Frederiksen, who provided all the necessary help I needed during my studies at the University of Manitoba. I will like to appreciate Dr. Ian Fergusson for his unending support towards my studies. My thanks also goes to Dr. Seth Stein (Northwest University) for his willingness to be a part of my examining committee.

I would like to thank Dr. Ademola Adetunji, who is a good friend and a senior colleague. My thanks also goes to Mulu Serzu, Taras Zaporazan and Brenda Miller for their advice and good wishes. My appreciation also goes to my colleagues and friends. Thank you all.

I would also like to thank my siblings and their spouses, Wole, Dele, Funke, Mayowa, Laitan and Sunday for their enormous support towards my studies.

Finally, I can't end this without acknowledging my wife, Opeyemi. She is always standing by me through the good times and the bad. You are indeed special.

Dedication

I dedicate this thesis to my parents, Solomon and Caroline Ola. They are the pillars behind my success. I love you both.

I also dedicate this thesis to my childhood friend and roommate during my Undergraduate program, Laolu, who lost his life in a ghastly motor accident during the course of his MSc. in Geophysics at the University of Lagos. Your death is still a shock to me.

Table of Contents

List of Tables

Table Page

List of Figures

Abstract

Seismic data from 31 seismic stations, consisting of 16 SPREE (Superior Province Rifting Earthscope Experiment) and 15 TA (Transportable Array) instruments located from 80 - 97°W and 41 – 55°N were used to measure the lateral variation in the lithospheric fabric beneath the Superior Province and the Mid-Continent Rift (MCR). I made shear wave splitting measurements of SK(K)S phases by using the eigenvector minimization approach of Silver and Chan (1991). Error surfaces for multiple events were stacked in back-azimuthal swaths to examine directional variability. A single anisotropic layer model is sufficient to explain my data.

My results show a high split time in the western Superior Province (WSP), very weak splits in the Nipigon Embayment and a moderate split in the eastern Superior. I observed low split times in the Penokean, Yavapai and Matzazal Provinces. A region of very low split is newly detected by this study immediately to the east of Lake Superior. The MCR shows moderate to low split times. There are subtle variations in the direction of the fast shear wave across the study region. The fast directions align with the direction of the absolute plate motion and the direction of tectonic boundaries in most regions.

Lateral variation of anisotropy and lithospheric fabric is observed across the study area. The strong fabric observed in the western Superior is truncated to its east and to its south. I interpret southward truncation to be due to the Mid-Continent Rift. My result shows that lithospheric fabric in the Nipigon Embayment (NE) located just east of the WSP has been lost or seriously modified. The NE is interpreted to be an hotspot feature, which may have initiated the MCR. Moreover, the result of this study suggests that the lithosphere in the MCR may have been thinned or modified though not as much as the lithosphere of the NE. The newly discovered

localized low split zone northeast of the MCR is similar in split time and extent to the feature in the NE. The relatively weak split in the eastern Superior Province may possibly be attributed to partial loss or modification of preexisting fabric resulting from the Great Meteor hotspot track.

CHAPTER ONE

INTRODUCTION

This research focuses on observing the strength and orientation of lithospheric fabric through measurements of the splitting of teleseismic SK(K)S waves at instruments in and near the Mid-Continent Rift (MCR) axis, a Proterozoic failed rift located in central North America.

Although the crustal expression of continental rifting is preserved after the rifting processes, it is impossible to determine from crustal evidence the nature of the lithospheric contribution to the rifting process (Stein et al., 2011). This brought about the installation of broad-band teleseismic instrumentation through the Superior Province Rifting Earthscope Experiment (SPREE) to allow investigation of the lithosphere beneath the MCR, which will help in addressing questions about the initiation, propagation, and failure of the rift structure.

Seismic imaging is a suitable method for detecting large-scale lithospheric mantle structures and for determining the degree to which they correlate with crustal terranes. High seismic velocity associated with stable continental lithosphere is often attributed to low temperature and depleted mantle, while low velocity features beneath cratons have in many places been attributed to hotspot activity heating, eroding or modifying the lithosphere (Frederiksen et al., 2007). Seismic anisotropy, the directional dependence of seismic wave velocity, is mostly of interest due to its link with deformational processes. Deformation in the Earth often results in seismic anisotropy (Long and Becker, 2010) because the deformation of mantle rocks often leads to the development of a preferred orientation of individual mineral crystals, thereby resulting in the directional dependence of seismic wave speeds (Long, 2013).

One of the two confirmed arms of the MCR extends southeastward from eastern Lake Superior to the southern boundary of Michigan, while the other arm extends from central Lake Superior to central Kansas. The Superior Province, especially the Lake Superior region, is of high importance to this research because the northern part of the MCR where the two arms meet is situated in the Lake Superior region. The Superior Province has been stable for about 2.6 Ga and is underlain by high velocity upper mantle (Godey et al., 2003). Frederiksen et al. (2007) suggested that there are lateral variations and small-scale high- and low-velocity structures within the region and a possible feature related to the Great Meteor hotspot.

1.1. Objectives of the study

The major aim of this research is to play a part in ongoing studies of what brought about the Mid-Continent Rift, to answer the question of why it ceased, rather than developing into sea floor spreading, and to contribute to overall understanding of the North American continent. This study investigates the effect of rifting on lithospheric fabric. Some of the things that will be addressed in this study include whether the lithospheric fabric was reset as a result of the rifting process, the degree of anisotropy variation and the influence of structures such as the Nipigon Embayment on the rifting process. This study will also allow us to compare previous tomography results in this region to shear wave splitting measurements.

The specific objectives of this project are:

- To determine the extent of anisotropy across the MCR – I used the results from teleseismic shear wave splitting parameters from SKS and SKKS to constrain the spatial variations of anisotropy across the MCR.

- To evaluate the extent of lithospheric thinning or modification – my results will also allow me to quantify the orientation and strength of mantle fabrics within our map region. The shear wave split time will show if the Mid-Continent Rift affected the full thickness of the lithosphere.

- To check for the possibility of multiple layers of anisotropy beneath the Mid-Continent Rift, which would indicate contrasting lithospheric/asthenospheric fabrics or lithospheric layering.

1.2. Significance of the Research

This research is important in the following ways:

- it will contribute to understanding North American tectonic history.
- it will help to better understand the role of lithosphere in the rifting process.

CHAPTER TWO

REGIONAL GEOLOGY

2.1. Introduction

North America is an amalgamation of tectonic provinces of different ages (figure 2.1). The continental core is Precambrian and includes two blocks that have been stable since the Archean: the Superior and Slave Provinces. In the mid-continent region, the target of this study, the Archean Superior Province abuts on Proterozoic blocks, including the Yavapai, Matzatzal, and Grenville Provinces and the Trans-Hudson and Penokean Orogens, all of which were affected by the Mid-Continent Rift (also known as the Keweenawan rift). In this chapter, I will briefly describe the nature and history of relevant geological regions. They will be explained in their order of accretion to ancestral North America.

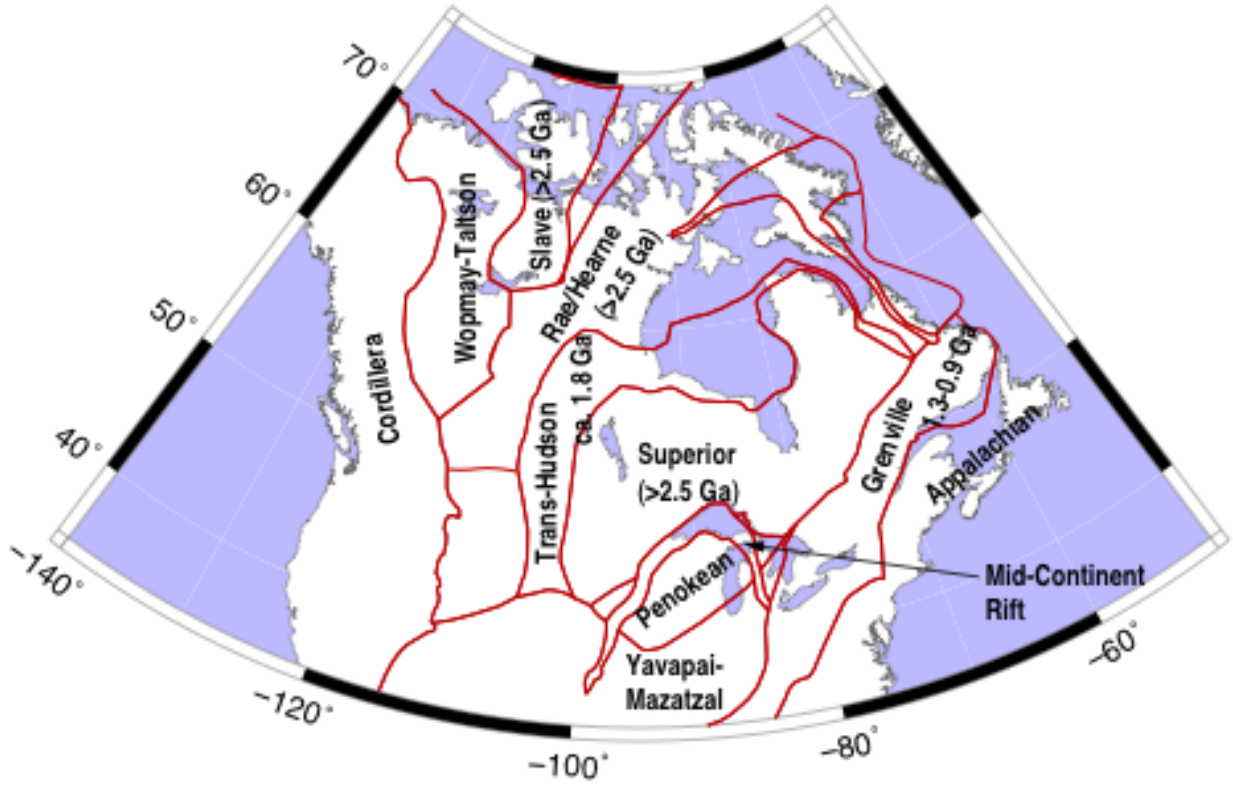

Figure 2.1: North American tectonic provinces. This shows the provinces discussed below as well as the location of the Mid-Continent (Keweenawan) Rift system. Boundaries are after Hoffmann (1988).

2.2. Superior Province

The Superior Province, about 2400 km wide, forms the nucleus of North America and is the largest preserved Archean crustal block in the world (Hoffman, 1990). The Superior Province is located in the south central part of the Canadian Shield and is believed to have its final form as the result of a widespread crustal accretion event (around 2.7 Ga) evident in Archean cratons worldwide (Kendall et al., 2002). This province has subdivisions that are very large and similar in size to major elements of modern orogenic belts (Card and Ciesielski, 1986). The major provinces that surround the Superior Province include the Grenville Province to the southeast,

the Trans-Hudson Orogen to the north and west, and the Penokean Orogen to the south. They are all categorized as Proterozoic orogenic belts (Darbyshire et al., 2007). The Minnesota River Valley Terrane (MRVT) is part of the Superior Province but not directly within the scope of this study. Studies (e.g Frederiksen et al., 2013b, Ferre et al., 2014) show that MRVT has seismic velocity characteristics that makes it different from the other Superior terranes.

There is little evidence of inheritance of components older than ca. 3.1 Ga in the middle and late Archean rocks of the Superior Province (Card, 1990), which are therefore interpreted to be juvenile crust origin. Late Archean greenstone successions exist all over the Superior Province, while middle Archean series are widespread in the north and central part of the Superior Province, but rare or absent in the south (Card, 1990). Thermotectonic events in the western Superior Province show a systematic north to south progression over a 40 million year time span (Percival et al., 2004). The importance of the Superior region is shown in the fact that it is the only region along the MCR where there is an exposure of volcanic rocks (Keweenawan group; Allen et al., 1992).

It is widely believed that mantle lithosphere beneath stable Archean regions such as the Superior province is of comparable age to the crust. Therefore, the Superior lithosphere is expected to preserve a record of subsequent thermal and tectonic events and should help in generating an historic record of rifting events (Frederiksen et al., 2013b).

2.3. Penokean Orogen

The mountain-building episode of the Penokean Orogeny occurred in the early Proterozoic at about 2 Ga, in what is now portions of Minnesota, Wisconsin, Michigan and Ontario. Schulz and Cannon (2007) note that the Penokean Orogeny is the oldest Paleoproterozoic accretionary

orogen along the southern margin of Laurentia and that it resides in an embayment along the southern margin of Archean Superior craton. The Penokean event ranged in age from about 1890 - 1830 Ma (figure 2.2). A basal quartzite in the Menominee Range, known as the Chocolay Group is the oldest preserved of exposed portion of the Penokean and was deposited in a rift basin with an extensive ocean between 2.3 and 2.2 Ga (Schulz and Cannon, 2007). This ocean began to close at about 1890 Ma (figure 2.2a), there was formation of the Pembine-Wasua oceanic arc in the east, while the Chocolay group and similar sediments continued to be deposited in the west.

At about 1.88 Ga, south-directed subduction ended and the Penokean Orogeny began when the Pembine-Wausau terrane collided with the southern margin of the Archean Superior craton (Schulz and Cannon, 2007). By 1875 Ma, the newly formed Marshfield Terrane was brought towards the south due to accretion of the Pembine-Wausau Terrane against the Superior craton in the east and a subduction flip, thereby resulting into the formation of a marginal arc and tholeiitic magmas (figure 2.2b). The end of the subduction coupled with closure of the ocean and collision of the Marshfield and Pembine-Wausau Terranes around the time of the Sudbury impact event in 1850 Ma, caused the deposition of ejecta into the foreland basin (Schulz and Cannon, 2007).

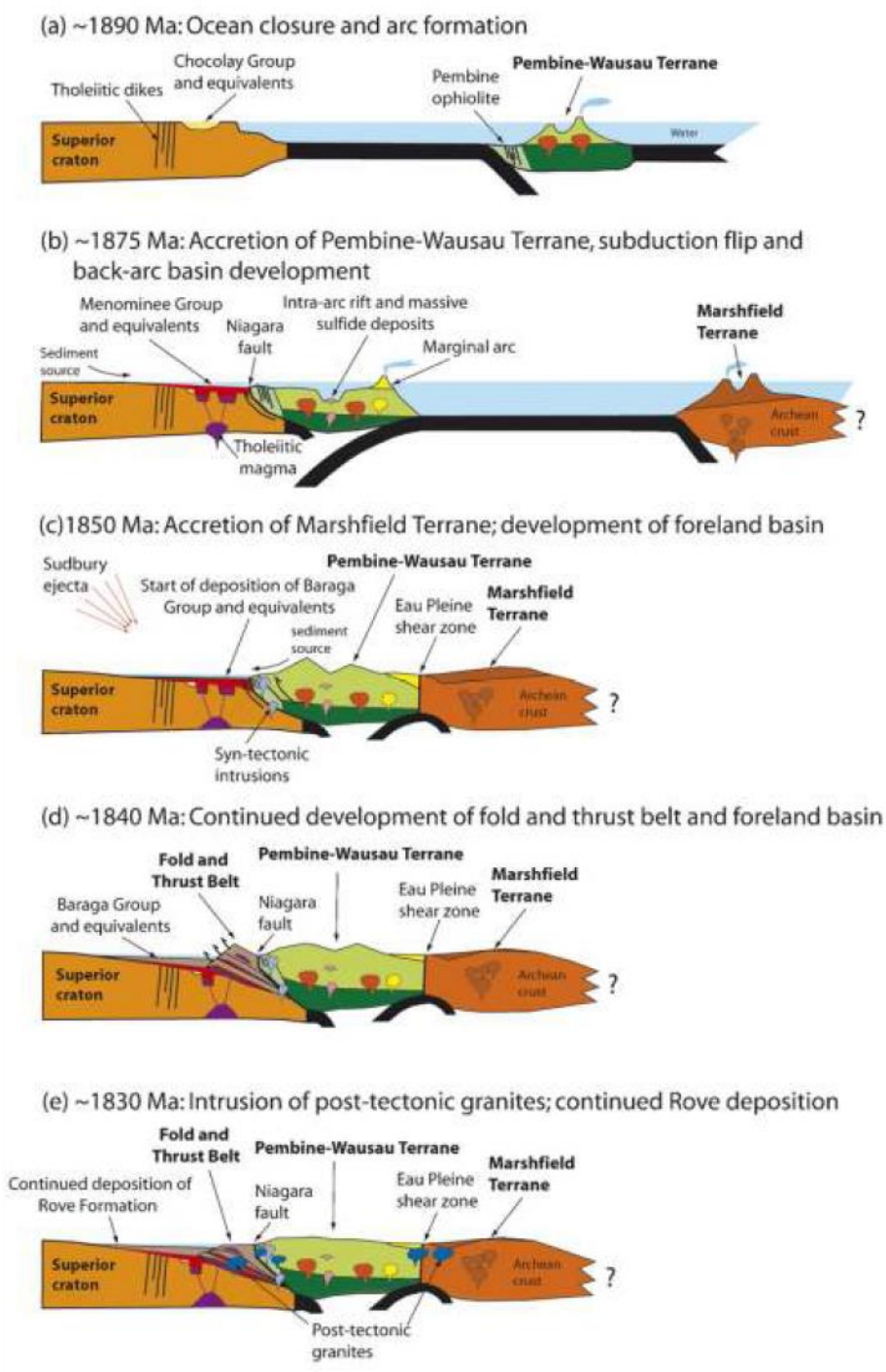

Figure 2.2: The stages of evolution of the Penokean Orogeny (Schulz and Cannon, 2007)

The Grenville orogen truncates the Penokean Orogen on the east, and the Penokean orogen is truncated on the southwest by the Central Plains orogen (Sims and Peterman, 1986). The rocks

from Penokean orogeny are poorly exposed around its segment in Minnesota. The southeastern region of the Penokean orogeny in Minnesota is tectonically complex and contains highly deformed sedimentary and volcanic rocks metamorphosed under varying conditions. In general, intensity of deformation and metamorphism of the Penokean increases from northwest to southeast (Southwick and Morey, 1991).

The Superior Province is truncated in the southeast by the overlapping effects of the Penokean orogen and the Mid-Continent Rift. Although the Penokean orogeny has been extensively overprinted by later tectonic activities such as formation of the Mid-Continent Rift (believed to be the largest source of overprinting), collision and continental growth occurring around 1.88 - 1.83 Ga in the southern margin of Laurentia are still well documented. Recent orogenic belts formed by plate tectonic processes are similar to structures and rocks formed during the Penokean orogeny (Van Schmus, 1976). The Penokean orogeny ceased around 1830 Ma and was marked by a suite of post-tectonic granite plutons.

2.4. Yavapai and Mazatzal Provinces

The Yavapai and Mazatzal Provinces represent different oceanic volcanic arcs that collided and accreted to North America. There are series of accreted arcs and continental-margin supracrustal rocks intruded by batholithic suites present in the Yavapai and Mazatzal orogens (Kalstrom and Humphreys, 1998). The formation and accretion of the combined Yavapai and Mazatzal Province occurred in about 150 million years (VanArsdale, 2009). Below are some of the notable points about the two terranes.

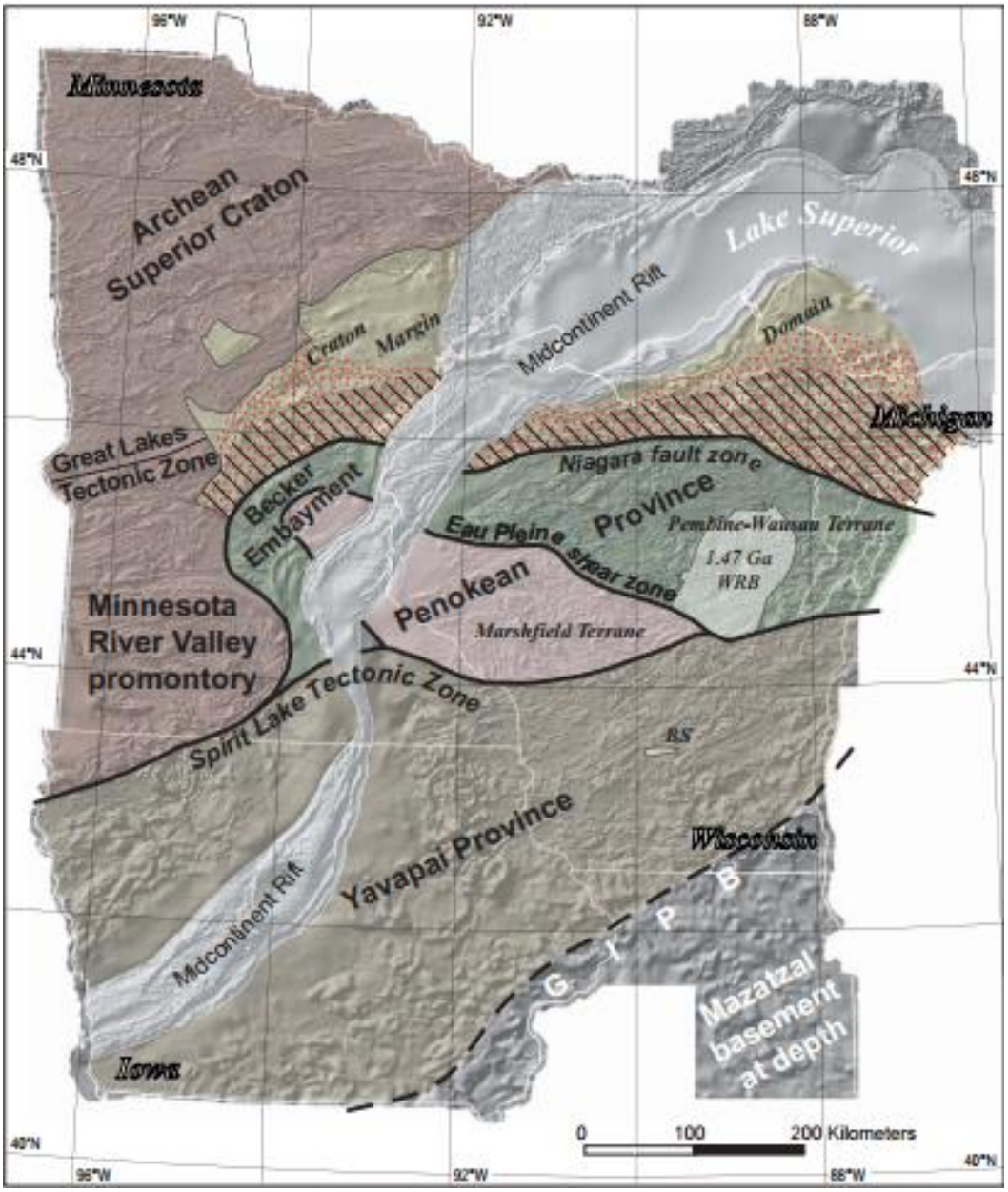

Figure 2.3: Geologic terrane map showing the Mid-Continent Rift and the basement rocks of some of the provinces described in this chapter (Holm et al., 2007)

2.4.1. Yavapai Province

The formation and accretion of the Yavapai Province took place between 1.8 and 1.7 Ga (McLelland et al., 1996) when juvenile crust was formed. This crust was subsequently deformed

during the 1.70 Ga Yavapai orogeny (Magnani et al., 2004). It appears that the Yavapai Province completed its accretion 1.7 Ga (Rogers and Santosh, 2004; Barth et al., 2000). The widespread syn-to early post-tectonic plutonism of this age seen all over the Yavapai Province can be traced to collisions on both sides of the Province at about 1.7 Ga (Condie, 1992). In the Southern Yavapai Province, northward-derived cratonic sediments were deposited within 20 Ma of the 1700 Ma collisions in some areas (Condie, 1992), consistent with the view that cratonization should commence within 30 million years of the end of collision (Thompson and Ridley, 1987).

The Yavapai Province consists of orthogneisses made up of tonalite, diorite, granodiorite and amphibolite, which are believed to have formed by partial melting of preexisting crustal rocks (Bickford and Hill, 2007). At around 1.76 - 1.72 Ga, the juvenile crust was formed and the Yavapai granitoids stitched regional terranes with older provinces (Schulz and Cannon, 2007). Quartzite deposition in the Yavapai occurred around 1.7 Ga. The 1.47 - 1.43 Ga granitic plutons, which are part of the "anorogenic" magmatism that transects a substantial part of the southern North American continent, are abundant in the Yavapai Terrane (Holm et al., 2007). A good understanding of the Yavapai Terrane is hindered by lack of information on its bedrock and poor geochronology control.

2.4.2. Mazatzal Province

The collision and accretion of the Mazatzal Province was between 1.68 and 1.65 Ga. The 1.68 - 1.65 Ga volcanogenetic greenstone successions, which include rhyolite, basalt and basaltic andesite, are believed to be the oldest rocks in the Mazatzal Province (Kalstrom et al., 2004). There is a greater abundance of granite in the Mazatzal Province than the Yavapai and it is believed to represent magmatic bodies that intruded the supracrustal rocks (VanArsdale, 2009).

The Eastern Granite-Rhyolite Province bounds the Mazatzal Province to the east. It is believed (e.g. Atekwana, 1996) that the Mazatzal Province rocks may continue beneath the Eastern Granite-Rhyolite Province. Melting of the underlying Mazatzal Province rocks may have possibly resulted in the granite and rhyolite in at least the western portion of the Eastern Granite-Rhyolite Province (VanArsdale, 2009).

The deformation of the 1.75 - 1.65 Ga Baraboo interval quartzites was associated with Mazatzal-aged tectonism in the mid-continent region (Whitmeyer and Karlstom, 2007). Holm et al., 2005 interpreted this in terms of accretion of the Mazatzal arc that resulted in south-verging folding of quartzites and the Penokean crust being mildly reheated. The Labradorian Orogeny (Dickin, 2000), an intense metamorphism and plutonism episode, was discovered to have taken place in Southern Labrador almost simultaneously with the Mazatzal Orogeny (Whitmeyer and Karlstom, 2007). Even though neodymium dating (ND) model ages (Van Schmus et al., 2007) suggests continuity through the Great Lakes-mid-continent region, the extent of Mazatzal-Labradonian crust in the mid-continent is still mostly undefined (Whitmeyer and Karlstom, 2007).

2.5. The Grenville Orogeny

The Grenville Orogeny was a Mesoproterozoic mountain-building event that ended in the formation of huge mountain range and the formation of supercontinent Rodinia. The formation of the Grenville Province at 1.3 - 1.0 Ga was a result of the collision of the North America craton with island arcs and then a continent to the east, which is believed to have either been carried away during the late Proterozoic and early Paleozoic opening of the Iapetus ocean or to have been buried beneath the Appalachian mountains (Atekwana, 1996). This collision is believed to

have occurred at about 1200 Ma. Associated granitoids intrude juvenile belts as far west as Colorado in 1.3 - 0.95 Ga (Whitmeyer and Karlstom, 2007).

The name "Grenville" is used only for events that occurred on the southern and eastern margins of Laurentia, even though orogenic crust of mid-late Mesoproterozoic age is found worldwide (Tollo et al., 2004). A plate collision ca. 1.1 Ga from south to north is believed to have resulted into the formation of the Grenville orogen in the Llano uplift and most probably eastward across the southern United States (VanArsdale, 2009). The main exposure of the Grenville Orogeny, one of the largest collisional orogen that is known in the world (Rino et al., 2008), is the Grenville Province. In Canada, the Grenville Province exposes mostly crystalline rocks and extends northeastward from Lake Huron to the coast of Labrador.

The boundary between the Grenville province and the older structural provinces to the northwest, the Grenville front (Wynne-Edwards, 1972), marks the northwestern limit of tectonic reworking of rocks of the older provinces during the Grenville orogeny and is distinct on regional gravity and magnetic maps (VanArsdale, 2009). The northwest-directed crustal-scale thrusting in the Grenville orogenic belt developed approximately simultaneously with the Mid-Continent Rift.

2.6. Mid-Continent Rift System

The Mid-Continent Rift system, also called the Keweenawan rift, is a 2000 km long rift zone that was initiated about 1.1 Ga in the stable interior of the North American craton (Stein et al., 2011). It is comparable in length to the presently active East African and Baikal rifts. The rift opened up, filled with up to 15 km of lavas (which solidified into basalt), and then the rifting ceased after about 15 - 22 million years of existence. Research has shown that many continental rifts fail to develop into seafloor spreading centres and thereby become an important part of the fabric of the

continents (Stein et al., 2011). The formation of this kind of rift, its failure to develop into an oceanic spreading center and its eventual stabilization remain ambiguous to researchers, despite the key role of failed rifts in shaping the fabric of the continents.

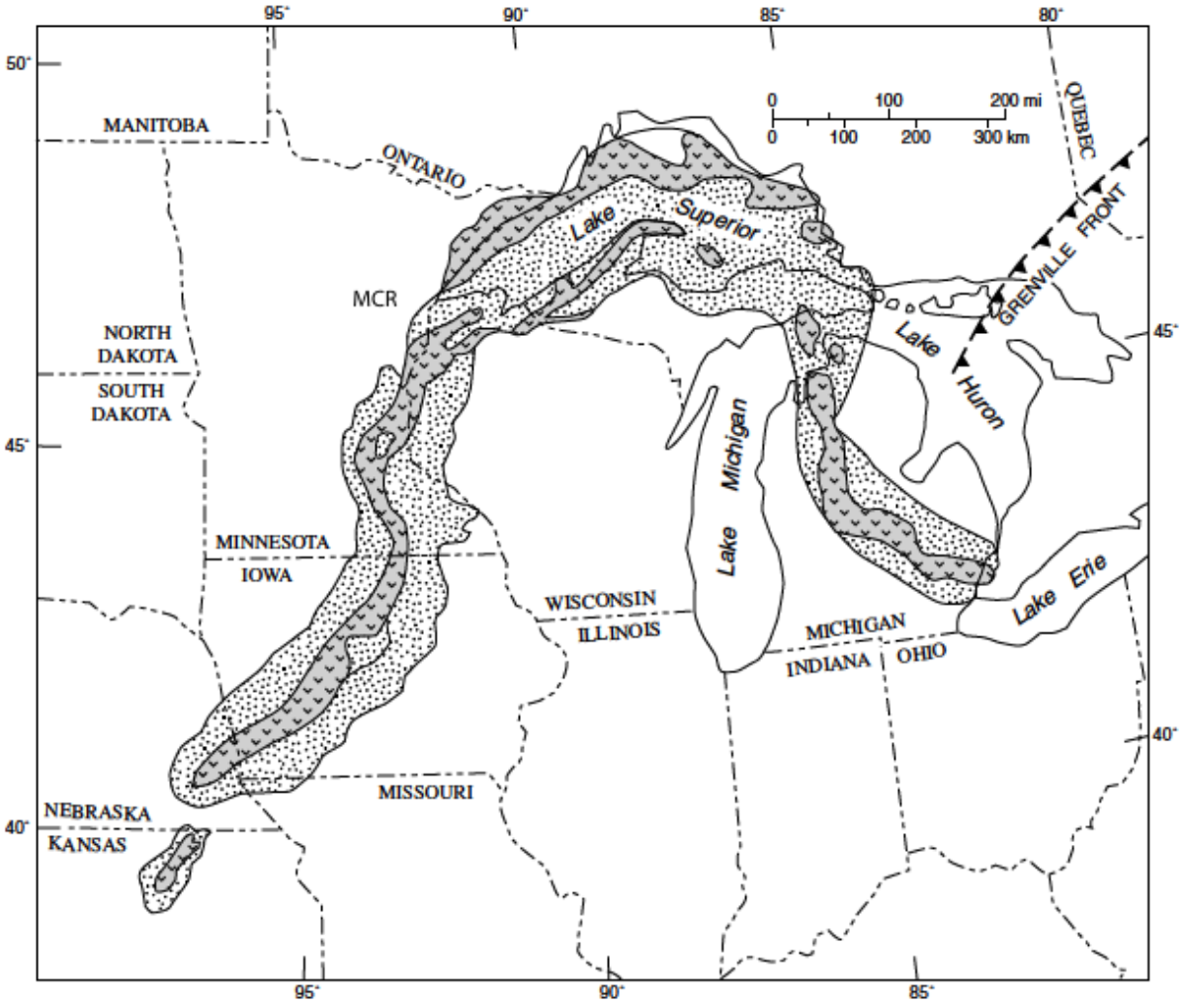

Figure 2.4: The Mid-Continent Rift system (Ojakangas et al., 2001)

Rifts are generally classified into active and passive rifts. This classification is usually based on whether there is thermal perturbation of the mantle causing disturbance in the overlying crust or there is plate interaction causing internal tension (Van Schmus and Hinze, 1985). In active rifting, the rifting process is driven by convective upwelling of the asthenosphere, while in

passive rifting, lithospheric extension and rifting are initiated and driven by horizontal, inplane far-field forces, possibly resulting from large-scale plate interactions (Huismans et al., 2001).

It was proposed by Ebinger and Sleep (1998) that active rifting in the East African Rift is a response to melting in the underlying asthenosphere or deeper mantle due to mantle plumes or shallower thermal or compositional anomalies. For the case of the Baikal Rift, where the Amurian plate diverges from Eurasia, rifting is described as a passive response to stresses transmitted within the lithosphere (Calais et al., 2003).

The Mid-Continent Rift system is considered to be primarily an active rift due to the large volumes of basaltic magmas associated with it and also because the Lake Superior basin, which forms a substantial part of the rift, is believed to be situated over a former hotspot (Van Schmus and Hinze, 1985). It is however vital to note that due to the proximity of the Grenville Province, it is possible that there is a significant contribution from extensional forces associated with a continental collisional zone to the development of the rift (Van Schmus and Hinze, 1985), which might also indicate a passive component. It is believed that due to widespread plate movement and breakup (as a result of frequent rifting around the world) during the time of occurrence of the Mid-Continent Rift, the rifting may be associated with a major extensional stress field that developed at this time in the continental lithosphere (Van Schmus and Hinze, 1985).

2.7. Nipigon Embayment

The Nipigon Embayment, formerly referred to as the Nipigon plate (Stockwell et al., 1972), is an inactive continental rift zone extending 160 km north from Lake Superior through the Wabigoon and Quetico subprovinces in Northwestern Ontario, Canada (Perry et al., 2004). The embayment is covered by mid-Proterozoic sediments intruded by Keweenawan diabase sills in the region of

Lake Nipigon north of Lake Superior (Sutcliffe, 1991). A series of east-trending greenstone belts that are separated by intrusive rocks of the central and eastern Wabigoon subprovince underlay most parts of the Nipigon Embayment (Hart and MacDonald, 2007).

Four main mafic to ultramafic intrusions have been identified in the Nipigon Embayment, namely the Seagull, Disraeli, Hele and Kitto intrusions (Hart and MacDonald, 2007). These intrusions include pyroxene, peridotite, iherzolite and wehrlite with irregular patches of monzogabbro and or pink feldspar along the contacts of the intrusions. Some mafic to ultramafic bodies are also present in the Nipigon Embayment, such as the Jackfish Sill which is about 10 - 60 m thick and believed to be of comparable age to the Mesoproterozoic ultramafic intrusions south of Lake Nipigon (Hart and MacDonald, 2007).

Contrary to previous suggestions (e.g. Franklin et al., 1980; Sutcliffe, 1991; Frederiksen et al., 2007) it has recently been proposed (e.g. Hart and MacDonald, 2007) that the Nipigon Embayment is not a failed arm of the Mid-Continent Rift. The main reason for this interpretation is the lack of extensional features in the Nipigon Embayment. For instance, recent geochronological studies (e.g. Heaman et al., 2007) showed that diabase sills and mafic-ultramafic intrusions around Lake Nipigon are the oldest expression of igneous activity associated with the Midcontinent Rift. The presence of sills rather than dykes suggests that the Embayment was not extensional during the Mid-Continent Rift. Moreover, Hollings et al. (2007) noted that since the initial formation of the Nipigon Embayment occurred at about 200Ma before the Mid-Continent Rift, and therefore the Nipigon Embayment cannot be a failed arm of the Rift. It is now suggested that structures of the Nipigon Embayment may have been associated with faults that were subsequently reactivated during the development of the Midcontinent Rift (Hollings et al., 2007).

CHAPTER THREE

REVIEW OF PREVIOUS GEOPHYSICAL STUDIES

3.1. Introduction

This chapter reviews the geophysical literature underlying my research and describes the progression of previous investigations. Many geophysical studies have been carried out to understand lithospheric structure and fabric across the Mid-Continent Rift and surrounding areas. In this chapter, I reviewed studies from different methods in the western Superior Province, Nipigon region and along the Mid-Continent Rift axis around Lake Superior.

3.2. SKS Splits

In order to characterize upper mantle anisotropy, core shear phases such as SKS and SKKS are commonly used (figure 3.1). The SKS phase is a useful way to obtain a plane-polarized S-wave at teleseismic distances. SKS and SKKS phases are detectable at distances between 90° and 130° from the epicenter**.** They propagate along steeply inclined ray paths between the core and the surface. The liquid nature of the outer core, and consequently the K-S conversion at the core-mantle boundary (CMB), produce an SV-polarized wave. SKS and SKKS are ideal for imaging tectonically stable regions because after phase conversion at the core mantle boundary, the shear waves propagate nearly vertically to the Earth's surface, forming isolated arrivals beyond 80° (Clitheroe and Van der Hilst, 1998). These teleseismic shear wave splitting phases provide valuable information on the dynamics and structure of the anisotropy of the Earth's upper mantle (Silver and Chan, 1991). Also, with SKS, the effects of anisotropy and lateral heterogeneity can be distinguished easily. Detailed examination of the SKS waveforms, as is done in the cross-

convolution method (Menke & Levin, 2003) can be used to diagnose multiple layers of anisotropy at depth.

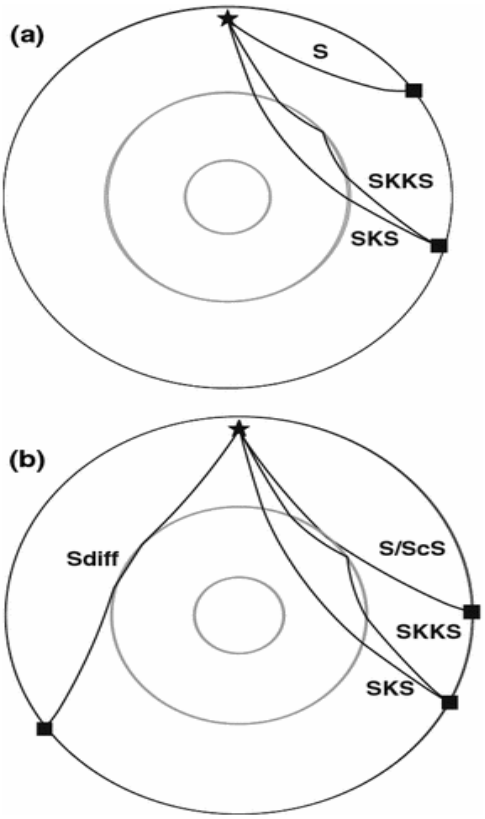

Figure 3.1: Phases commonly used to probe mantle anisotropy (Long and Silver, 2009)

3.3. Seismic Anisotropy

Seismic anisotropy refers to the variation of the velocity of seismic waves with direction of propagation and polarization. It was recognized some decades ago by seismologists that regions of the Earth's mantle are anisotropic (e.g., Hess 1964; Forsyth 1975), but lately the presence of seismic anisotropy has been observed in many environments and at many depths in the Earth, from the crust down to the core-mantle boundary. The presence of seismic anisotropy at several depth ranges in the mantle is now established (Long and Silver, 2009). The dominant source of

anisotropy in shear-wave splitting appears in the upper mantle. This is believed to be a result of the disappearance of olivine at the 410 km discontinuity. Olivine is anisotropic and does not exist below 410 km, where it is eliminated by a phase change reaction. Mantle anisotropy is predominantly observed in the upper mantle; and seems not significant in the mid-mantle, though there may be some in the D" region. Many seismologists study anisotropy in the upper mantle due to its likely connection with past and present geodynamic processes (e.g., Silver, 1996).

Seismic anisotropy is believed result from deformation in the Earth through lattice preferred orientation (LPO) of anisotropic constituent minerals or through the shape preferred orientation (SPO) of materials with distinct isotropic elastic properties (Long and Becker, 2010). A common source of SPO is aligned cracks. Because anisotropy in the mantle is generally attributed to deformation, measurement of seismic anisotropy is an excellent tool to directly probe patterns of deformation at depth. The main sources of upper mantle anisotropy are olivine and pyroxene LPO that are acquired through plastic flow (Ferre et al., 2014). Measuring anisotropy remotely from the Earth's surface is therefore a way to access present or past mantle flow at depth.

The ease of use and the potentially powerful interpretations makes the shear-wave splitting technique, a phenomenon where a shear wave splits into two orthogonally polarized s-waves whenever it encounters an anisotropic material, stand out among methods employed in detecting upper-mantle anisotropy. Shear wave splitting measurements can characterize the orientation and depth extent of mantle strain fields (Savage, 1999), allowing researchers to examine structural geology within the mantle.

3.4. Western Superior Mantle Anomaly

The Western Superior Mantle Anomaly (WSMA) is a term introduced (Frederiksen et al., 2013b) to refer to a region of strong anisotropy coinciding with a high-velocity zone in the Superior Province. The WSMA is believed to be a locus of an unusual lithospheric fabric with a coherent WSW-ESE direction. This region is interpreted to as a preserved fabric from the accretion of the Superior Province. The Trans-Hudson Orogeny marks the boundary of the western Superior to the southwest, while the Mid-Continent Rift marks its boundary to the southeast. The position of the western edge of the WSMA at about 200 km east of the crustal contact with the Trans-Hudson orogen suggests that the processes involved in the accretion of this orogen eroded the Superior lithosphere (Frederiksen et al., 2013a).

To better understand the accretionary processes active during the Archean, knowledge of the velocity structure of the upper mantle beneath the Western Superior Province (WSP) is required (Sol et al., 2002). The WSP is unusual in many ways. First, it is associated with large SKS splitting while the surrounding Trans-Hudson orogen shows weaker splits. It also shows thicker than usual Archean crust and the presence of a slab-like velocity anomaly in the transition zone (Kendall et al., 2002).

Studies showing this unusual anomaly in the western Superior go back a few decades. Silver and Kaneshima (1993) identified a strong E-W fabric along the western border of Ontario; a further study along a north-south line west of Lake Nipigon (Kay et al, 1999) confirmed this result. Further studies with areal arrays (Frederiksen et al., 2007, 2013b) show an average split time between the fast shear wave and slow shear wave of more than 1 s in the western Superior Province, with the largest value found being about 1.8 s.

Tomography results by Frederiksen et al. (2007, 2013a) showed a high velocity anomaly in the Western Superior bounded by low velocity lithosphere to the east (figure 3.2). This is consistent with the shear wave splitting analysis result in this region (e.g. Frederiksen et al., 2007 and 2013b), which shows a high shear wave split in the western Superior. A smaller-scale study by Sol et al. (2002) located significant velocity anomalies in the WSP. Their investigation based on inversion of P- and S- wave travel times suggests the presence of a dipping tabular high-velocity anomaly and two low velocity features.

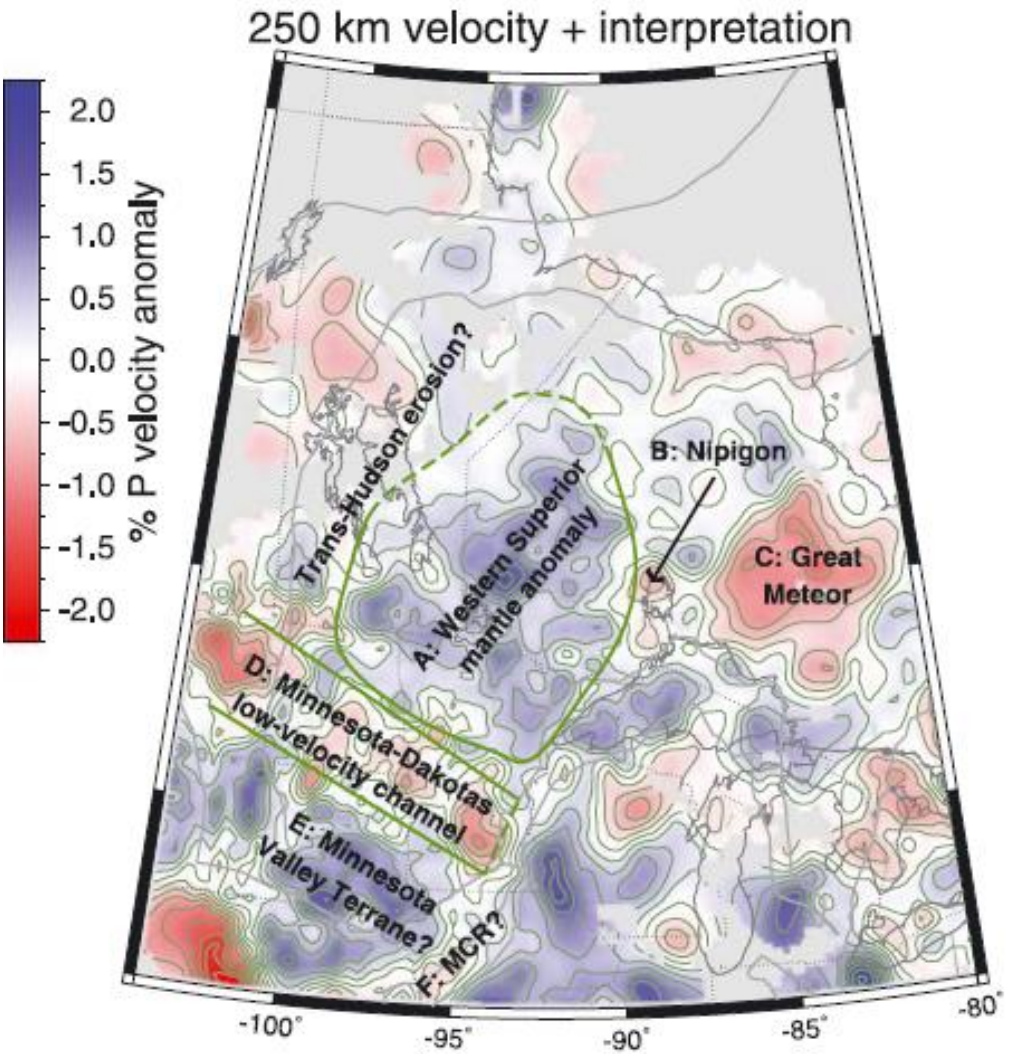

Figure 3.2: Tomography results at 250 km showing the velocity anomaly beneath different structures (Frederiksen et al., 2013a)

Magnetotelluric soundings of Ferguson et al. (2005) also show a Western Superior that is somehow distinct to neighbouring regions. They identified a dominantly east-west geoelectric strike at long periods (except in the North Caribou and Wawa subprovinces that have older lithosphere) and also an isolated linear east-west striking conductive anomaly.

3.5. The Mid-Continent Rift System

The SKS data set used by Frederiksen et al. (2013b) only had limited coverage of the southern Minnesota and northern Iowa axis of the mid-continent rift, other parts of the rift axis being unsampled. They suggest that possible thinning or modification of the lithosphere beneath the MCR and its replacement by less-depleted mantle material may have caused a difference in the lithosphere beneath the MCR and the surrounding continental material. Even though the study of Frederiksen et al. (2013b) has poor coverage of the Mid-Continent Rift, the authors detected a low velocity feature via tomography (Frederiksen et al., 2013a), which made them tentatively suggest that the Mid-Continent Rift affected the full thickness of the crust and the continental lithosphere.

Although most parts of the rift axis have not been well studied in previous studies using shear wave splitting analysis, SPREE seismic stations will help me improve resolution of these regions in this study. This is described in more detail in chapter 5.

3.6. The Nipigon Embayment

The Nipigon Embayment is another important structure in this region, which is believed to have been involved in the Mid-Continent rifting process. The Nipigon Embayment is a magmatic region (Hart and MacDonald, 2007) located at the eastern edge of the western Superior and north of Lake Superior. It displays extensive crustal magmatism, approximately of the same age as the MCR or slightly older, and an associated mantle anomaly seen in both seismic tomography and magnetotellurics (Ferguson et al., 2005; Frederiksen et al., 2007). From the evidence of the Nipigon lithospheric anomaly, it was also suggested that anomalous upper mantle may underlie

the MCR assuming that Nipigon Embayment shares a common origin with the MCR (Frederiksen et al., 2013a).

Generally, this region appears as a low velocity anomaly structure using seismic tomography measurements (see figure 3.2). Frederiksen et al. (2007) suggested that the slow anomaly identified by the tomography measurements of Sol et al. (2002) underlies the Nipigon Embayment.

This mantle anomaly beneath the Nipigon Embayment is also evident in magnetotelluric studies (Ferguson et al., 2005). Magnetotelluric soundings at more than 230 sites in the western Superior Province detected an anomalous phase response beneath the Nipigon Embayment. In Lake Nipigon around the Superior Province, the dimensionality results show that the general behaviour is three-dimensional, especially at longer periods (deeper penetration). However, results from the Nipigon Embayment show one-dimensional structure at short periods (shallow penetration). This MT result implies that a layered crust in this region is underlain by three-dimensional mantle. This suggests that Proterozoic tectonic processes affected the resistivity of the whole crust and the underlying mantle.

CHAPTER FOUR

METHODOLOGY

4.1. Introduction

Measuring shear wave splitting robustly gives the strongest evidence for anisotropic wave propagation (Evans et al., 2006). Due to greater availability of seismic data as a result of the increasing age and number of permanent networks and temporary seismic stations across the globe (Butler et al., 2004), studies using shear wave splitting to measure mantle anisotropy have become more common.

Most studies of upper mantle anisotropy now analyze splitting of seismic phases that transit the Earth's core, such as SKS and SKKS (Silver and Chan, 1991). Because the incident polarization of these waves is always known to be SV, we can regard the presence of energy on the SH component as evidence for anisotropy. In order to understand upper mantle anisotropy beneath Japan, Ando and Ishikawa (1982) were the first to use splitting observations in vertically travelling phases, while Vinnik et al., (1984) started the use of observations of shear wave splitting in teleseismic core-transiting phases (Evans et al., 2006).

One of the main challenges that can be encountered in shear wave splitting measurements is the possibility of multiple layers of anisotropy, which results in systematic variations of shear wave splitting parameters with azimuth. The shear wave splitting parameters measured in the presence of two anisotropic layers and the analysed assumption of a single layer approach will give apparent parameter results that will show azimuthal variation (Evans et al., 2006).

Three methods are commonly used in obtaining shear wave splitting parameters; the transverse energy minimization method, the eigenvalue method (Silver and Chan, 1991), and the cross correlation method (Bowman and Ando, 1987). The transverse energy minimization method and the eigenvalue method, which are applicable to single-layer anisotropic models; are used in this project. For multilayer anisotropy, other methods may be used for shear wave splitting such as the cross-convolution method of Menke and Levin (2003), which is briefly described later in this chapter. How both methods are used in our research will be discussed in chapter 5, but this chapter will describe the theory underlining these methods.

4.2. Shear wave splitting

Similar to birefringence in optics, shear wave splitting occurs when a seismic shear wave travels through an anisotropic layer (Wustefeld et al., 2009**)**. Shear waves are similar to electromagnetic waves in that they may adopt a range of different polarizations perpendicular to the travel direction, and can be considered a sum of two orthogonally-polarized wave modes. In isotropic materials, the two shear modes have equal velocities, but in anisotropic materials, their velocities differ. On encountering an anisotropic region, a single linearly polarized shear wave pulse will split into two quasi-shear waves of different velocities (figure 4.1), which become separated in time as the wave travels. In shear wave splitting analysis, the direction of the fast wave, ϕ, and the delay time between the two shear waves, δt, are important. These are referred to as the shear wave splitting parameters. The delay time measured at the Earth's surface between the two split waves depends on the strength of the anisotropy and on the thickness of the anisotropic layer.

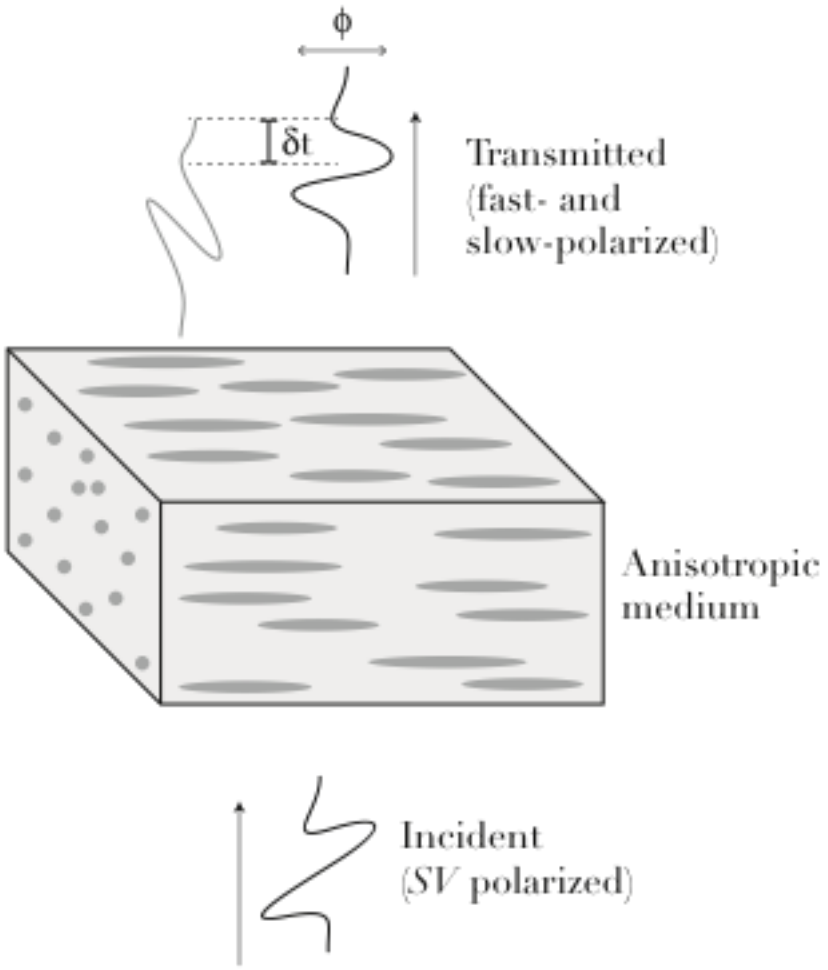

Figure 4.1: Shear wave travelling through an anisotropic medium

Mean global split times in the oceanic lithosphere and stable cratonic lithosphere are on the order of 0.5 - 1.5 s and 1 s respectively (Silver, 1996). It is generally considered that split times larger than 0.5 s will require significant mantle anisotropy (Savage, 1999). Savage (1999) suggested that split times greater than 2.0 s cannot be generally explained with the anisotropy confined to the upper mantle above 220 - 250 km. Delay times less than 0.5 s are difficult to measure by classical data analysis techniques and are commonly considered to be null measurements (Chevrot et al., 2004). These null measurements are often interpreted as the presence of an

anisotropic layer that is too thin to be detected, or of an anisotropic layer with a sub-vertical symmetry axis.

4.3. Shear wave splitting identification problems

In some situations, shear wave splitting may not be identified by splitting methods, as briefly discussed in this section.

4.3.1. Null measurements

Null measurement is a term used when the incident shear wave is linearly polarized and there is an absence of transverse energy, indicating no apparent splitting of the incoming shear wave (Savage, 1999). Null measurements show either the absence of significant horizontal anisotropy (isotropy) or that the initial polarization matches the fast or the slow axis (Wustefeld and Bokelmann, 2007). In such conditions, measurements of the splitting parameters are unstable. In most shear wave splitting studies, null measurements are considered separately (e.g. Silver and Chan, 1991; Fouch et al., 2000) or neglected (Wustefeld and Bokelmann, 2007), though they may be included in error surface stacks.

There are different ways in which null and non-null measurements are identified. These include the coherence of the waveform between fast and slow directions, the signal to noise ratio on the transverse component, the elliptical shape of the particle motion before correction and the linearity of the particle motion after correction (Barruol et al., 1997). Although these approaches are commonly used, they have limitations in near-null directions, in which it is hard to make a consistent and reproducible classification (Wustefeld and Bokelmann, 2007). There are cases that resemble a null, such as observations of small splitting delay times in weak anisotropic media over short distances (Saltzer et al., 2000).

Wustefeld and Bokelmann, (2007) used the eigenvalue method (Silver and Chan, 1991) as well as the rotation correlation method to detect null measurements and their quality. They detected nulls by examining the difference between the fast direction of these two methods and the ratio between the two delay times. This method was improved by Wustefeld et al. (2010) to detect the quality of nulls, which allows us to differentiate measurements that appear null (due to noise) from genuine nulls (Walsh, 2013).

4.3.2. Cycle Skipping

Cycle skipping is a phenomenon in which the first trough of the slow waveform fits the first peak of the fast waveform (Matcham et al., 2000), leading to delay time measurements that are incorrect by some integer multiple of half of the dominant period. This situation can be expressed mathematically by;

$$\delta t_{CS} = \delta t \pm nT/2$$

where δt is the true delay time, δt_{CS} is the cycle skipped delay time, T is the dominant period and n is a positive integer (Walsh, 2013).

This occurrence leads to errors in the shear wave splitting parameters because there will be matching of the wrong peak of the waveform or matching of a peak with a trough (Walsh, 2013). We observe cycle skipping when the amplitude of the peak of the wave is small (Matcham, 1997). Because cycle skipping shows up as multiple minima on error surfaces, error-surface stacking over many events can help in addressing this problem.

4.4 Complex anisotropy (multiple layers of anisotropy)

Measured splitting parameters (fast direction, ϕ, and delay time, δt) in the presence of multiple layers of anisotropy cannot be simply related to the geometry of any one layer as the analysis assumes single, laterally homogeneous layer of anisotropy with a horizontal axis of symmetry (Silver and Long, 2011). For a homogenous medium, the relation between the splitting parameters, the fast polarization direction φ and delay time δt, and the elastic tensor C_{ijkl} is straightforward even for more general anisotropy. This relation can become somewhat complicated for multiple regions of anisotropy, but the assumption of a localized homogeneous anisotropic layer seems to be justified in most cases (Silver, 1996). In the presence of multiple anisotropic layers, the apparent splitting parameters will vary with polarization direction. Multiple layers of anisotropy with different symmetry axes can cause unusual effects on splitting parameters because each split phase will split again as it propagates through subsequent layers. In the top anisotropic layer, whatever shear phases arrive will again be split into fast and slow components, and the initial wave polarization will be parallel to the fast direction of the last layer of anisotropy traversed (e.g., Yardley and Crampin, 1991).

When different measurement methods are used for splitting analysis, the discrepancies in the measured apparent splitting parameters are interpreted as an important diagnostic for the presence of complex anisotropy at depth. Complex anisotropy will result in correspondingly complex waveforms that do not conform to the predictions of the single horizontal layer of anisotropy (Menke and Levin, 2003).

Many methods have been used to extract information about complex anisotropy. One is Forward modeling studies that try to match observed splitting patterns with predicted ones. Other

techniques used for predicting apparent shear wave splitting parameters for complex anisotropic structures include those that employ particle motion (e.g., Fischer et al., 2000) and those based on pseudospectral waveform simulations (e.g., Chevrot et al., 2004). Inverse modeling (shear wave splitting tomography) is also used for this purpose (Chevrot, 2006, Long and Silver, 2009).

Another method that could be used for shear wave splitting analysis of a multiple-layer anisotropic model is the cross-convolution method. Menke and Levin (2003) proposed this method to address the possibility of complex anisotropy at depth. The method involves convolving the observed radial and tangential component seismograms with the opposite-component impulse responses predicted by a hypothetical Earth model, and varying the model to minimize the misfit between observed and predicted seismograms. In the presence of single horizontal layer of anisotropy, the cross-convolution method gives a similar result to commonly used one-layer methods. However, this method allow for multiple layers and may do a better job in distinguishing whether complex anisotropic models are required for a particular data set (Long and Silver, 2009).

4.5 Transverse energy minimization method

The transverse energy minimization method is among the most commonly used splitting measurement methods for broadband data. This method, first introduced by Silver and Chan, (1991) utilizes a grid search approach to identify the pair of splitting parameters (ϕ, δt) that best minimizes the amount of energy on the transverse component when the effect of splitting is accounted for. The principle employed in this method is to reverse the effect of splitting in order to retrieve the original wave. The shear wave splitting parameter pair that selected as the solution best removes the effect of splitting.

Many assumptions are made in this method. Firstly, it assumes a single layer of anisotropy (Walsh, 2013) and transverse isotropy with a horizontal axis of symmetry (Chevrot, 2000). Furthermore, it is assumed that there is no initial energy on the transverse component so the particle motion caused by the incoming isotropic wave is linear with SV polarization (Vecsey et al., 2008).

The transverse energy minimization method builds upon the fact that the polarization of shear waves is linear in an isotropic medium, but becomes elliptical when it passes through an anisotropic medium (Long and Silver, 2009). This situation can be represented mathematically.

Suppose that the incident wave, w_o is a sinusoid:

$$w_o = A_o\cos(\omega t)\mathbf{r} \quad (1)$$

where **r**: unit vector in radial direction (SV polarized)

Now, reproject onto the **f**, **s** unit vectors (fast and slow directions, assumed orthogonal);

$$w_o = A_o\cos(\omega t)((\mathbf{r}\cdot\mathbf{f})\mathbf{f} + (\mathbf{r}\cdot\mathbf{s})\mathbf{s}) \quad (2)$$

or

$$w_o = A_o(\mathbf{r}\cdot\mathbf{f})\cos(\omega t)\mathbf{f} + A_o(\mathbf{r}\cdot\mathbf{s})\cos(\omega t)\mathbf{s} \quad (3)$$

Now delay the slow wave relative to the fast wave to obtain the split waveform w_s:

$$w_s = A_o(\mathbf{r}\cdot\mathbf{f})\cos(\omega t)\mathbf{f} + A_o(\mathbf{r}\cdot\mathbf{s})\cos(\omega (t - \delta t))\mathbf{s} \quad (4)$$

and rotate back:

$$w_s = A_o(\mathbf{r}\cdot\mathbf{f})(\mathbf{f}\cdot\mathbf{r})\cos(\omega t)\mathbf{r} + A_o(\mathbf{r}\cdot\mathbf{f})(\mathbf{f}\cdot\mathbf{t})\cos(\omega t)\mathbf{t} + A_o(\mathbf{r}\cdot\mathbf{s})(\mathbf{s}\cdot\mathbf{r})\cos(\omega (t - \delta t))\mathbf{r} + A_o(\mathbf{r}\cdot\mathbf{s})(\mathbf{s}\cdot\mathbf{t})\cos(\omega (t - \delta t))\mathbf{t} \quad (5)$$

indicating that w_s contains a non-zero **t** component. If β is the angle between **r** and **f**, then:

$$\mathbf{r} \cdot \mathbf{f} = \cos\beta,\ \mathbf{r} \cdot \mathbf{s} = -\sin\beta,\ \mathbf{t} \cdot \mathbf{f} = \sin\beta,\ \mathbf{t} \cdot \mathbf{s} = \cos\beta \quad (6)$$

and so,

$$w_s = A_o\cos^2\beta\cos(\omega t)\mathbf{r} + A_o\cos\beta\sin\beta\cos(\omega t)\mathbf{t} + A_o\sin^2\beta\cos(\omega\,(t - \delta t))\mathbf{r} - A_o\cos\beta\sin\beta\cos(\omega\,(t - \delta t))\mathbf{t} \quad (7)$$

and

$$w_s = A_o(\cos^2\beta\cos(\omega t)) + \sin^2\beta\cos(\omega\,(t - \delta t)))\mathbf{r} + A_o(\cos\beta\sin\beta(\cos(\omega t) - \cos(\omega\,(t - \delta t)))\mathbf{t} \quad (8)$$

where $A_o(\cos^2\beta\cos(\omega t)) + \sin^2\beta\cos(\omega\,(t - \delta t)))\mathbf{r}$ is the radial component of the split shear wave and $A_o(\cos\beta\sin\beta(\cos(\omega t) - \cos(\omega\,(t - \delta t)))\mathbf{t}$ is the transverse component. The transverse component is zero if $\delta t = 0$. If $\delta t \neq 0$ and we plot the particle motion over a cycle, it forms an ellipse. A consequence of this situation is that energy on the transverse component of a shear wave becomes significant in an anisotropic material. Moreover, for SKS phases, the energy on the transverse component is minimized when the splitting effect is removed.

It is however worth mentioning that a small delay time, a small angle between the fast axis direction and the polarization direction, or a significant level of noise will result in a small amount of energy above the noise level on the transverse component, thereby poorly constraining the shear wave splitting parameters (Restivo and Helffrich, 1999). The problem of low signal to noise ratio can be compensated for by a stacking technique (Wolfe and Silver, 1998). I used the error surface stacking technique in this work to compensate for azimuthal variation in my measurements, as discussed in section 4.7 and in chapter 5.

4.6 Eigenvalue Minimization Method

The eigenvalue minimization method, also known as the standard correction method (Silver and Chan, 1991), is a familiar tool in extracting polarization and delay time information from split seismograms. This approach is a slight variation on the Transverse Energy Minimization method. The major difference is that it involves minimizing the smaller eigenvalue of the corrected covariance matrix, which is equivalent to creating the most linear particle motion (Long and Silver, 2009), instead of minimizing the energy on the transverse component as in the transverse energy minimization method.

The eigenvalue method is carried out by performing a grid search over all the possible values of ϕ and δt in a defined time analysis window. The horizontal components are rotated by ϕ and time-shifted by δt. The result with the lowest second eigenvalue of the corrected particle-motion covariance matrix has the most linear particle motion after correction and is the solution which best corrects for the splitting. The covariance matrix will have only one non-zero eigenvalue if anisotropy is completely removed from the system. However, if noise is present, there will be two eigenvalues in the covariance matrix, with the second eigenvalue corresponding to a measure of the amount of noise in the system (Walsh, 2013).

It is required that the corrected waveforms in the analysis window match after the splitting correction has been applied. The second eigenvalue of the particle-motion covariance matrix provides a measure of this match, and so the smaller the second eigenvalue, the better the match (Teanby et al., 2004).

One major advantage of the eigenvalue minimization method over the transverse energy minimization is that the transverse energy minimization is prone to error if the polarization of the

incident wave is not exactly the same as the backazimuth (as could arise for a ray deflected by mantle velocity anomalies) while the eigenvalue minimization is not. The eigenvalue approach finds the most linear polarization direction, even if it is not the SV direction. This also means that it is applicable to plane S waves in some cases.

4.7 Comparison between the two methods

4.7.1 Similarities

The similarities between the transverse energy and the eigenvalue minimization methods include:

1. both give similar results in a single layer anisotropic model.
2. both assume that the particle motion before splitting is linear (Walsh, 2013).
3. both assume that the ray is near vertical (Walsh, 2013).

4.7.2. Differences

The major differences between the two methods are enumerated below

1. The eigenvalue minimization method is more susceptible to cycle skipping for a moderate signal to noise ratio (S/N) compared to the transverse energy minimization method (Vecsey et al., 2008). This is because the periodicity of the eigenvalue minimization method is half the periodicity of the transverse energy minimization method. This cycle-skipping can be removed by shortening the maximum time lag (δt) interval.
2. The use of the transverse minimization method is limited to core-mantle refracted waves (polarized linearly in the ray-path plane), while the eigenvalue method can be

employed for shear waves with a more general linear polarization (Vecsey et al., 2008).

3. The eigenvalue method can be employed in situations where the initial polarization is not known, unlike the transverse method (Savage, 1999).

4.8 Error Estimation and Stacking

4.8.1 Error Estimation

The Fischer test (commonly referred to as an F-test analysis) is used to obtain a 95% confidence interval for the optimum values of the shear wave splitting parameters. This method is preferred because it is computationally inexpensive (Silver and Chan, 1991).

Bootstrap analysis is an alternative for calculating errors in ϕ and δt (Sandvol and Hearn, 1994). The advantage of the bootstrap method is that it is free of assumptions relating to the distribution of data errors or model parameters (Efron and Tibshirani, 1991) and can be used to control and check the stability of results, because bootstrap analysis results are asymptotically more accurate than using sample variance and assumptions of normality (DiCiccio and Efron, 1996). It is, however, more computationally expensive than the F-test.

4.8.2 Error Surface Stacking

Stacking of error surfaces is an essential component in shear wave splitting analysis. This is important in order to obtain a shear wave splitting parameter result close to the true mean value in the presence of azimuthal variation at each of the recording stations, and to reduce the effect of noise on single-event measurements. No matter the method used, noise is always something to

worry about in measurements because splitting measurements involve comparing both radial and transverse component waveforms, which are noise contaminated (Monteiller and Chevrot, 2010).

Different authors (e.g. Restivo and Helffrich, 1999) have identified shortcomings in the two methods described in this chapter in noisy environments. Consequently, Wolfe and Silver (1998) introduced stacking of error surfaces to improve the robustness of the two methods. They proposed that in noisy environments, stacking techniques can be employed to minimize the errors in the calculation of the splitting parameters. This may be achieved by stacking the error surfaces of different events with varying incoming polarizations (Montellier and Chevrot, 2010). This error surface is simply the grid of error values from the grid search for a single event. Error maps obtained by stacking different events usually give a robust estimate of splitting parameters (Monteiller and Chevrot, 2010).

In this work, I build on the previous studies by stacking the error surfaces twice. I first stacked individual events in 10° backazimuthal swaths (figure 7.1), and then stacked the individual swath stacks with equal weighting (see more in chapter 5 of this thesis). This is done to equalize the effect of different backazimuthal values on the stack (Frederiksen et al, 2007).

CHAPTER FIVE

DATA AND ANALYSIS

5.1. Introduction

In spring 2011, geoscientists from American and Canadian universities, including Northwestern University, Washington University in St. Louis, University of Minnesota, University of Manitoba and Université du Québec à Montréal, installed a series of seismometers in Minnesota, Wisconsin, and Ontario (figure 5.1) in the context of the Superior Province Rifting Earthscope Experiment (SPREE). The seismometers were deployed until fall 2013 and recorded earthquakes that occurred locally, regionally and all over the world. The data extracted from these recordings will be used to produce high-resolution images of the Earth's interior below the area (Stein et al., 2011).

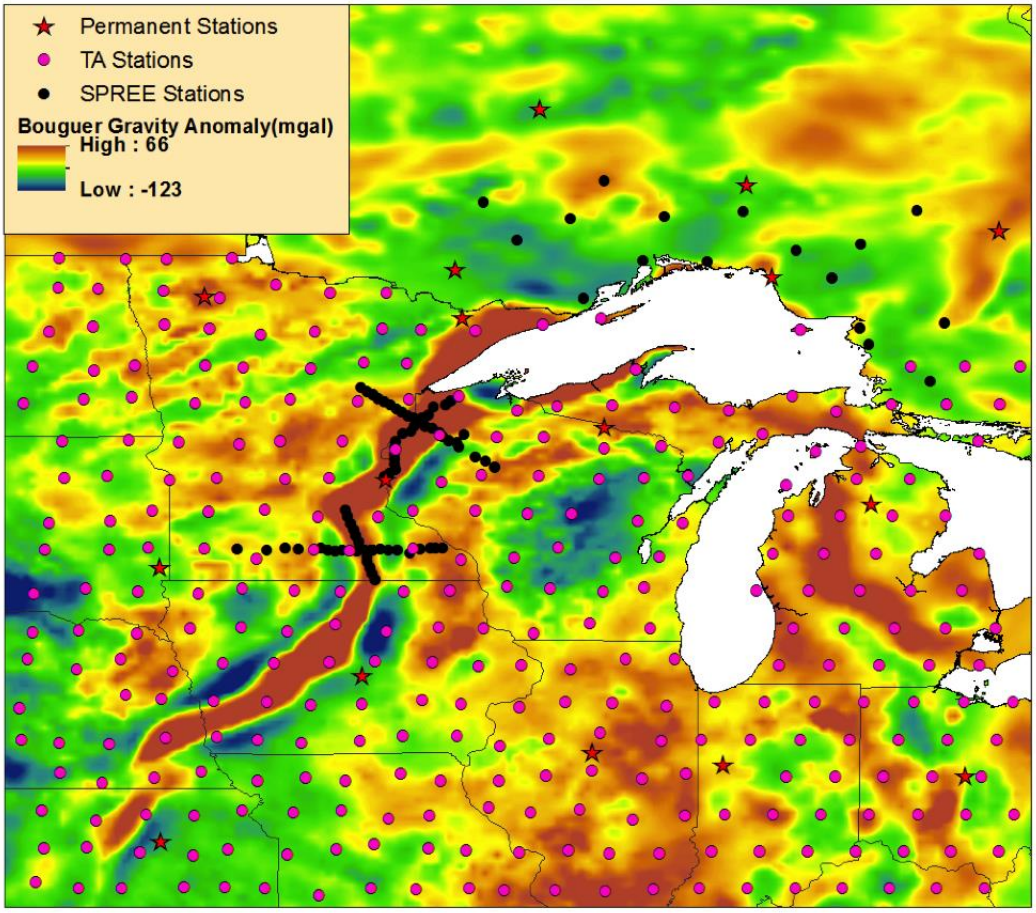

Figure 5.1: The distribution of seismic stations in the study area (central North America). The red stars represent permanent stations, purple circles are Transportable Array stations (15 of them are used in this research), while the black circles represent SPREE stations (the SPREE stations to the north of the border represent the 16 Canadian stations used in this research). The high gravity anomaly indicates the location of the Mid-Continent Rift (Stein et al. 2011).

Sixteen SPREE stations were placed north of Lake Superior in Ontario. These stations were installed in areas where there is little noise generated by cars, trains, and occupied buildings. The stations were fenced with nets to prevent animals from damaging the buried seismometer and electronics box. The electronics were powered by solar panels (figure 5.2) and enclosed in a plastic box covered with a polythene tarp to avoid water penetrating into the box. The stations

were serviced twice a year, mostly around May and October. The servicing runs were necessary to allow us to retrieve data, put the stations in proper order, check for possible infiltration of water into the electronic components after the winter season and to check if the battery was still being charged by the solar panel. At this time, damaged components were changed and seismic data were collected.

Figure 5.2: A typical Canadian SPREE station with its seismometer and electronic box buried underground.

Data recorded by the seismometers were stored on a memory card which was pulled out and replaced with an empty memory card during servicing. These data were checked, collated and

sent to the Incorporated Research Institutions for Seismology (IRIS), data management centre that archives and distributes data to support the seismological research community.

I made my analysis using all sixteen of the Canadian SPREE stations and fifteen Transportable Array stations (figure 5.3). These stations were chosen due to their proximity to the Superior Province and the axis of the Mid-Continent Rift, which are the target areas for this work. My choice of stations was also oriented to sample areas not covered by previous studies; portions of the MCR to the west were previously sampled by Frederiksen et al. (2013b).

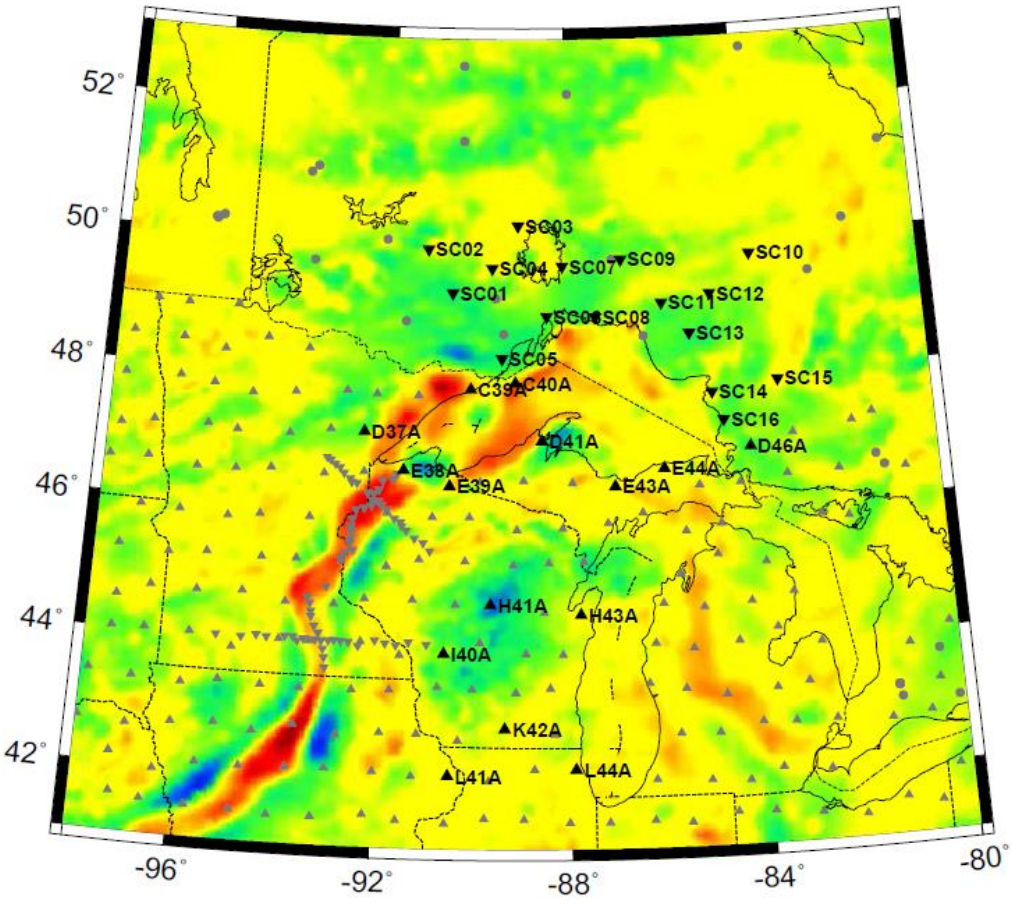

Figure 5.3: Seismic stations used in this project (black triangles). Background is Bouguer gravity.

5.2. Data acquisition

The data used in this research were acquired from the Incorporated Research Institutions of Seismology (IRIS) data base. The SeismiQuery page of the IRIS website (http://www.iris.edu/SeismiQuery/) was used to locate stations within a particular region. Since my target area is around Lake Superior, I chose all 16 Canadian SPREE stations, SC01 – SC16, and 15 nearby Transportable Array stations, which include C39A, C40A, D37A, D41A, D46A, E38A, E39A, E43A, E44A, H41A, H43A, I40A, K42A, L41A and L44A. Seismic events recorded by these stations were used for the analysis.

I used the ANSS earthquake catalogue website (http://quake.geo.berkeley.edu/anss/) to get a full list of the events that occurred later than January 1, 2011 with a minimum of magnitude 6. To obtain SKS pulses free from interference, I picked events in the 90° to 130° distance range from a target latitude and longitude, which is equivalent to 10000.8 km and 14445.6 km respectively (since 1° = 111.12 km). The latitude and longitude chosen (47.79, -87.70) correspond to a point at the centre of Lake Superior. The distance range chosen is at which the SKS is expected not to overlap with other arrivals.

A script is used for sending the data request via email. This script specifies all the parameters and an email response is received between one and three days later, depending on the availability of the requested data. The data generally come in a SEED archive and are then converted to SAC files before processing.

5.3. Selection

Upon the arrival of the data, I separated the data into different stations using a shell script. The Tau-P Toolkit (Crotwell et al., 1999) was used to predict the SK(K)S arrival times, which were added to the data header. I also ensured a good quality data by removing noisy seismograms from further analysis. This quality control was fairly time consuming but worth it. On average, about 40% of the events for each station were retained for analysis.

5.4. SK(K)S Arrival Picking

The picking process involves choosing windows containing the SK(K)S arrivals. It is preferable to do this manually (visually) as I did it in this work. Although visual inspection and picking of the wave arrivals is time consuming, it gives me more confidence in my results.

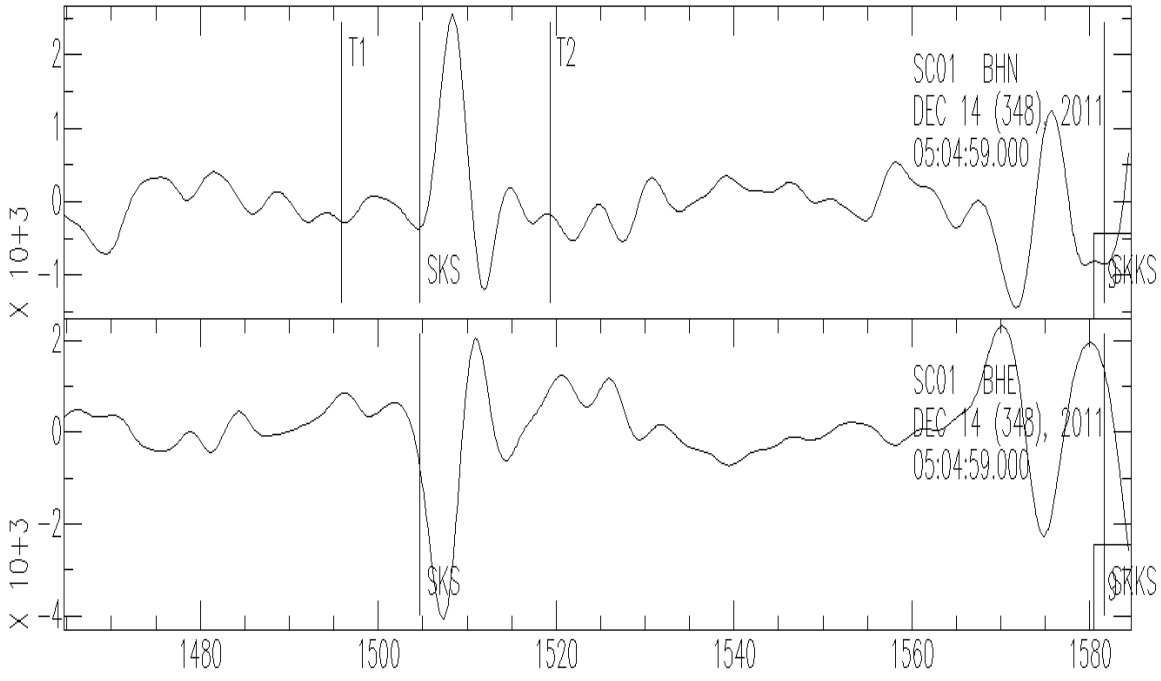

Figure 5.4: SKS arrival picking. The range between the T1 and T2 marks is the selected window.

The window around the predicted arrival time on the seismogram was selected using the SAC picking interface (figure 5.4). The window bounds are chosen by trying to completely enclose a pulse believed to be SKS or SKKS, and exclude any other arrivals. An elliptical particle motion within this window signifies the presence of anisotropy.

A common problem with both eigenvalue minimization and transverse energy minimization approaches is that the calculated shear wave splitting parameters, ϕ and δt, are sensitive to the choice of shear wave analysis window. Invariably, selection of the shear wave analysis window is subjective and can significantly influence the result.

5.5. Splitting Analysis

The shear wave splitting analysis was done using the same MATLAB routine as Frederiksen et al., (2007). Those commands yield plots showing the shear wave splits obtained using two approaches, the eigenvalue minimization method and the transverse energy minimization method.

Using the transverse energy minimization approach, the energy on the transverse component is minimized and the particle motion becomes corrected to linear from its elliptical form. This is obvious in Figure 5.5 (the top centre and bottom centre boxes show the input and the corrected particle motion respectively). In the input box there is substantial energy in the transverse component (upper right) that has been minimized in the corrected particle motion (lower right).

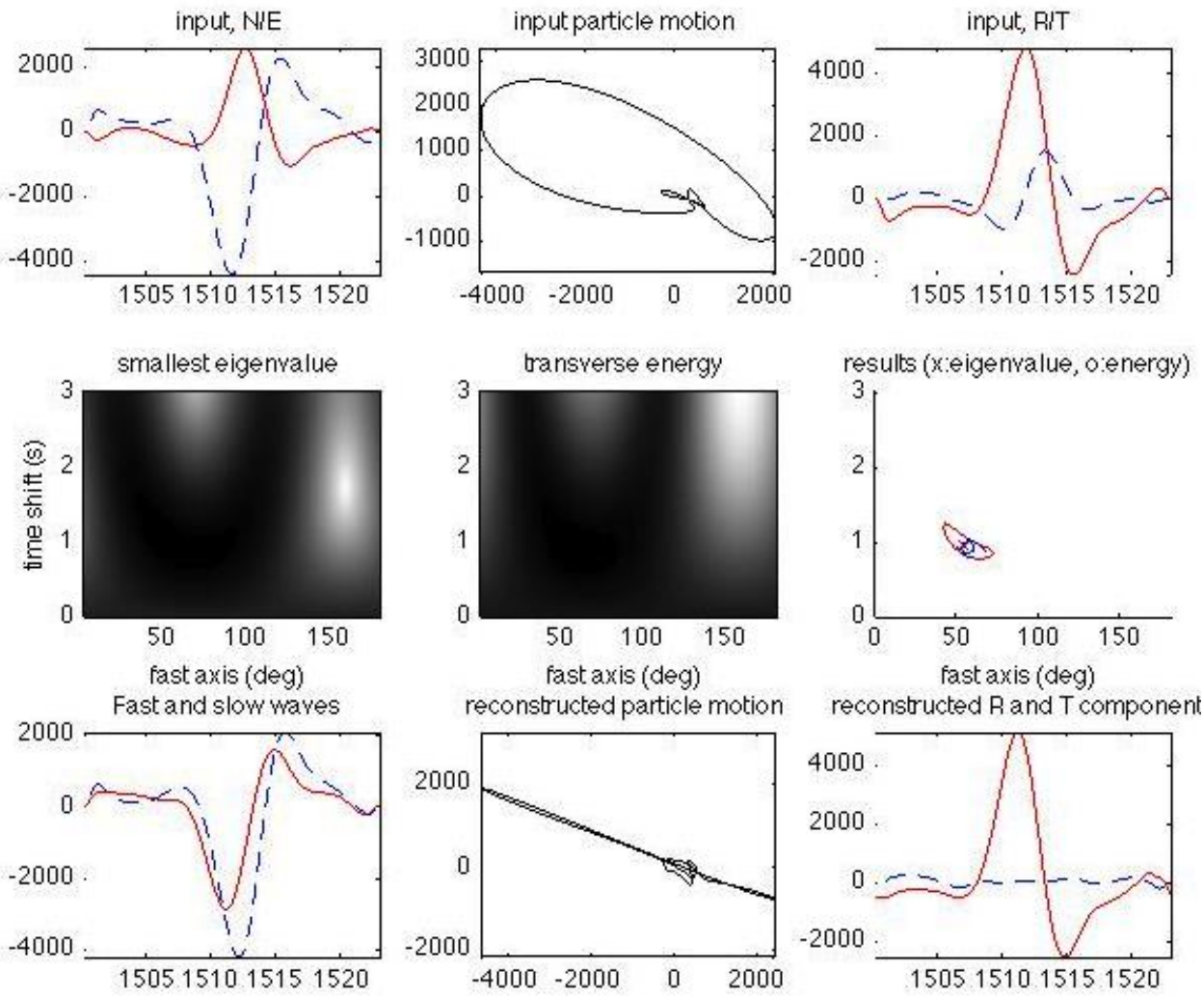

Figure 5.5: SKS arrival splitting results from event 20111214.050459 recorded by SPREE station SC05, located near the rift axis, using the eigenvalue minimization and the transverse energy minimization methods (Silver and Chan, 1991).

For the eigenvalue method, the script selects the set of shear wave splitting parameters for which the particle motion is most linear after processing. Both transverse energy minimization and eigenvalue method should give the same result if the incident wave is SV polarized. The eigenvalue minimization method was the only method retained for my final measurements, so it is the only method I will consider in my interpretation. However, I used the transverse energy

minimization method to check consistency of my results. The results from both methods are not significantly different, which gave me more confidence in the values I plotted on the splitting map.

The output box displays the confidence region (centre right panel in figure 5.5). The output plot shows the 95% confidence interval from the F-test, obtained from the error surfaces shown in the centre left and middle panels. Referring to the centre left and middle panels in figure 5.5, we can observe that the error surfaces from both methods are similar in appearance. This could be seen as evidence of the accuracy of my result.

5.6. Stacking

The next step is stacking all the events at a particular station to obtain a high quality estimate of the shear wave splitting parameters. The stacking process is done in two stages. First, I stack error surfaces from each of the events in 10° back azimuthal swaths (figure 7.1). I then stack events in the swaths with equal weighting (figure 5.6), to compensate for the dominant influence of swaths with high seismicity. I double stack my events because if too many events come in from the same direction, that direction will dominate. The double stack reduces this problem, and allows inspection of back-azimuthal variations to check for multilayered effects.

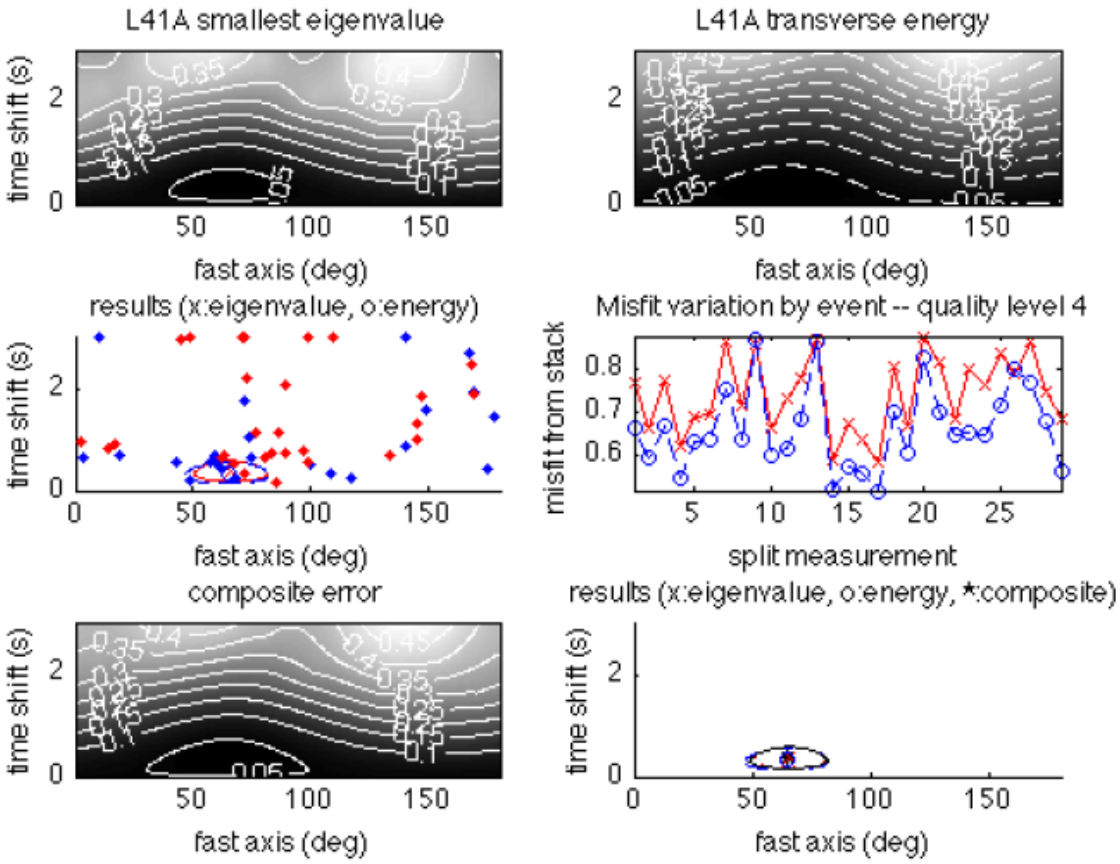

Figure 5.6: composite stacking of events with quality 4 at station L41A

5.7. Quality Control

The events analysed are also put under quality control after the splitting analysis. This is done is by giving qualitative rankings based on a number of factors such as signal to noise ratio, linearization of particle motion, and magnitude of the final ϕ and δt estimates. I consider the estimates successful when the corrected particle motion is linearized from its elliptical form and when the energy on the transverse component is significantly minimized. I ranked the measurements on a scale from 5, the best-quality events, to 1, the worst estimate. The example in figure 5.5 is assigned quality '5' because it is one of the best measured events. These are

tabulated and saved in a separate folder. Below are samples of the splitting results that I graded in this project (figures 5.7 to 5.10).

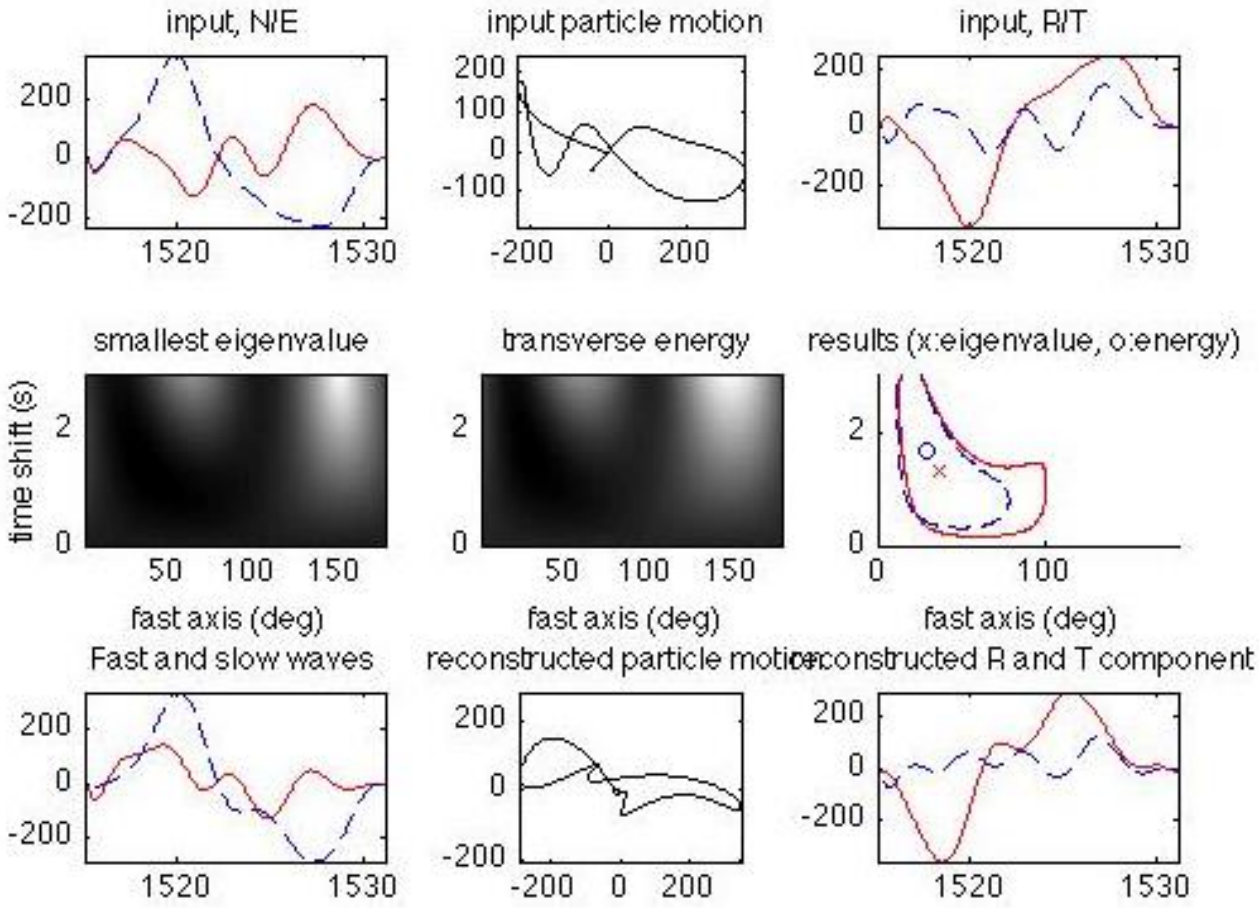

Figure 5.7: Quality 1 - station SC10, event 20110621.020415

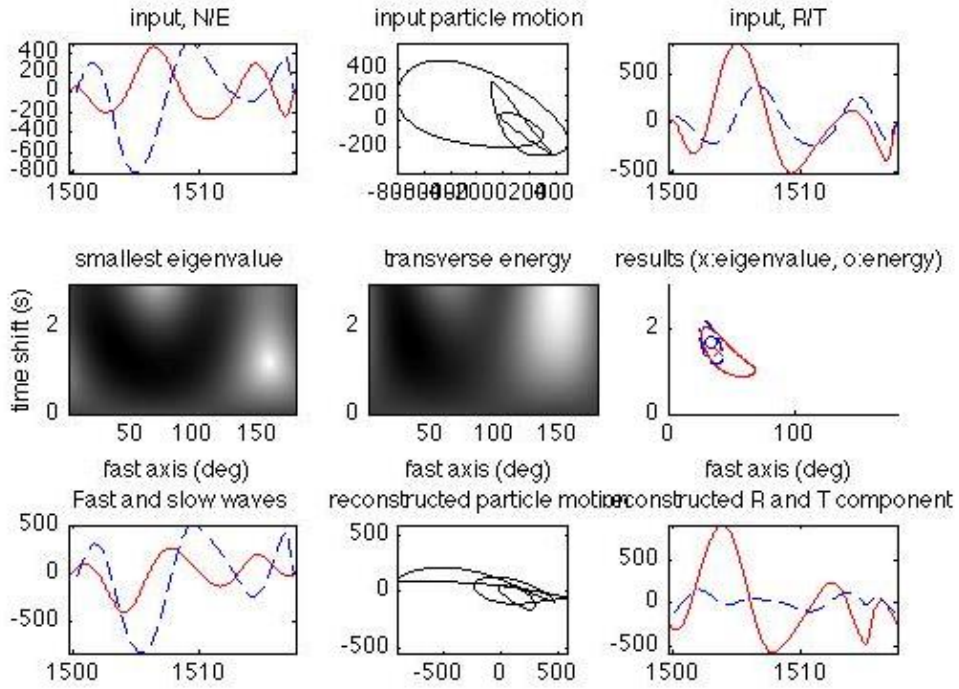

Figure 5.8: Quality 2 - station SC05, event 20120214.081955

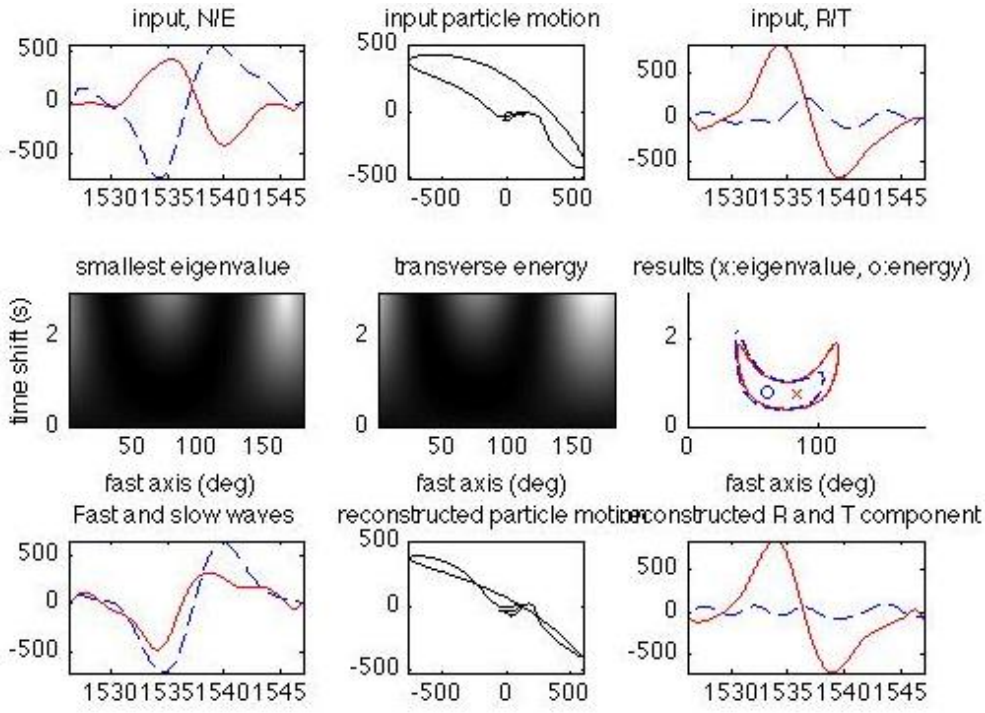

Figure 5.9: Quality 3 - station SC04, event 20130416.225527

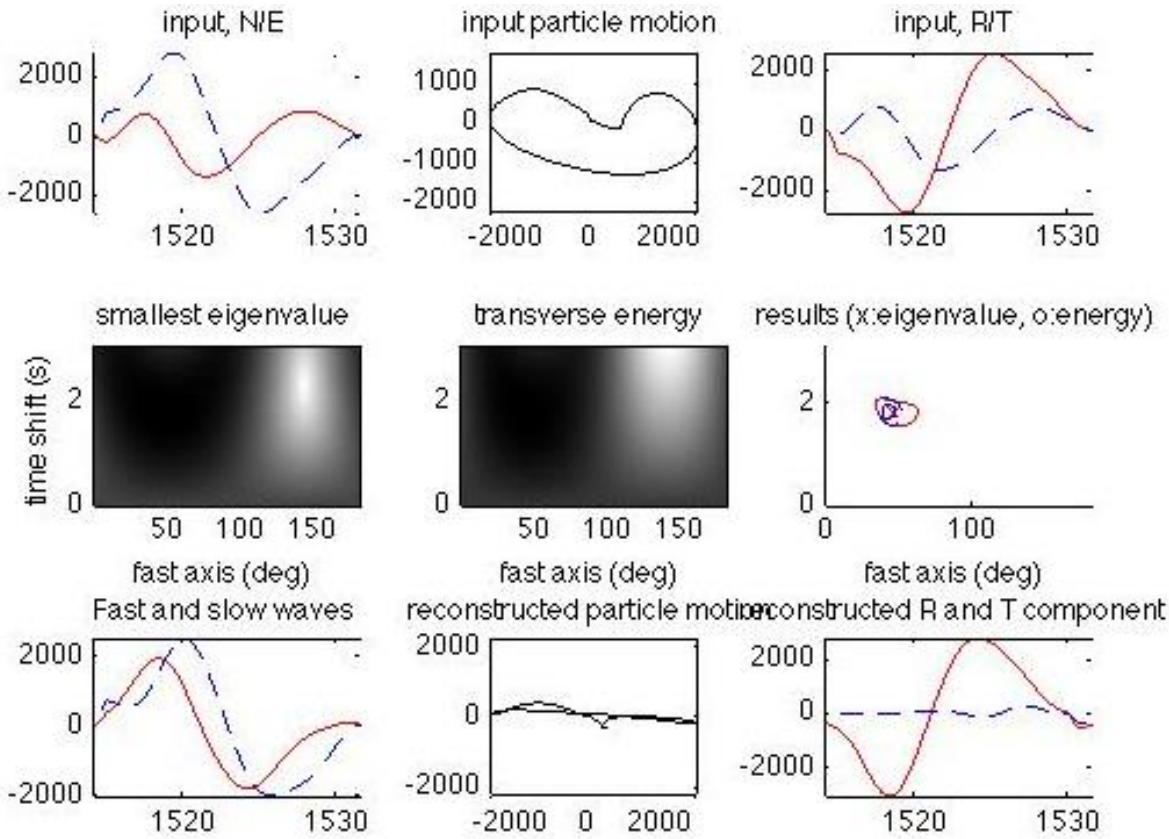

Figure 5.10: Quality 4 - station SC05, event 20130208.152638

The quality levels determined for individual events were used as a criterion in the stacking step. For stacking purposes, I only used results of quality 3 and above and ignored lesser quality measurements. This will be discussed in chapter 6.

CHAPTER SIX

RESULTS

6.0. Introduction

During the research, I analysed data from 31 seismic stations (16 Canadian SPREE stations and 15 Transportable Array stations). I received more than 2500 events within a 2-year time frame (May, 2011 to June, 2013) from the IRIS Data Management Centre. For these events, I detected 1734 SKS arrivals and 1735 SKKS arrivals while all other events were discarded because the SKS and SKKS arrivals were not visible. Due to my stringent quality measures, I used only 543 SKS and 347 SKKS traces for the final analysis. These events are of quality '3' or greater. Results of my shear wave splitting analysis are shown in figure 6.1 and table 6.1 and will be discussed in this chapter.

Table 6.1 shows the station name, latitude, longitude, final shear wave splitting parameter estimates and their errors for each of the seismic stations investigated. In these results, there are three null results (where the error is close to or greater than the split time, so zero or very weak splitting is possible) at stations SC07, D46A and K42A.

Station	Latitude	Longitude	ϕ(degrees)	+/- ϕ	δt(seconds)	+/- δt
SC01	49.2500	-90.5680	74	11	0.85	0.33
SC02	49.8950	-91.1410	66	8	1.48	0.35
SC03	50.2540	-89.0940	68	19	0.78	0.38
SC04	49.6240	-89.6750	75	10	0.90	0.25
SC05	48.2800	-89.4430	64	10	0.85	0.28
SC06	48.9050	-88.4460	67	31	0.43	0.35
SC07	49.6510	-88.0880	67	28	0.25	0.20

SC08	48.8880	-87.3570	73	17	0.45	0.23
SC09	49.7400	-86.7550	80	12	0.75	0.30
SC10	49.7530	-83.8170	74	13	0.93	0.28
SC11	49.0840	-85.8560	89	11	0.73	0.25
SC12	49.1890	-84.7630	61	12	0.83	0.25
SC13	48.6130	-85.2580	70	8	0.90	0.23
SC14	47.7230	-84.8140	81	23	0.38	0.25
SC15	47.8610	-83.3540	62	25	0.40	0.33
SC16	47.3050	-84.5880	80	17	0.40	0.23
C39A	47.817100	-90.12890	66	12	0.55	0.18
C40A	47.915400	-89.15140	58	10	0.55	0.20
D37A	47.16	-092.43	40	19	0.58	0.25
D41A	47.060500	-88.56570	36	19	0.33	0.20
D46A	46.89	-084.04	107	41	0.28	0.33
E38A	46.605800	-091.5542	58	16	0.78	0.30
E39A	46.3777	-90.55557	50	10	0.60	0.20
E43A	46.375800	-86.99540	61	8	0.88	0.25
E44A	46.619900	-085.9214	71	11	0.58	0.25
H41A	44.6164	-089.6534	65	12	0.53	0.23
H43A	44.4697	-087.7704	79	12	0.63	0.33
I40A	43.8916	-090.6177	86	16	0.48	0.25
K42A	42.7792	-089.3457	86	33	0.25	0.20
L41A	42.0751	-090.4977	66	16	0.38	0.23
L44A	42.1782	-087.9119	68	17	0.45	0.28

Table 6.1: shear wave splitting parameter results and errors for 16 SPREE seismic stations and 15 Transportable Array stations

The splitting map (figure 6.1) shows the values from the table, plotted as red arrows. The length of the arrow is the time lag between the two quasi-S waves while the direction of the arrow shows the orientation of the fast shear wave. The arrows are centred on the locations of the

corresponding stations. I added previous splitting measurements (black and grey arrows) to check for consistency and to see a overview of anisotropy within the Superior Province. I also produced contour maps of the individual splitting parameters (figures 6.2 and 6.6) which provide a clearer view of the spatial variation of the shear wave splitting parameters.

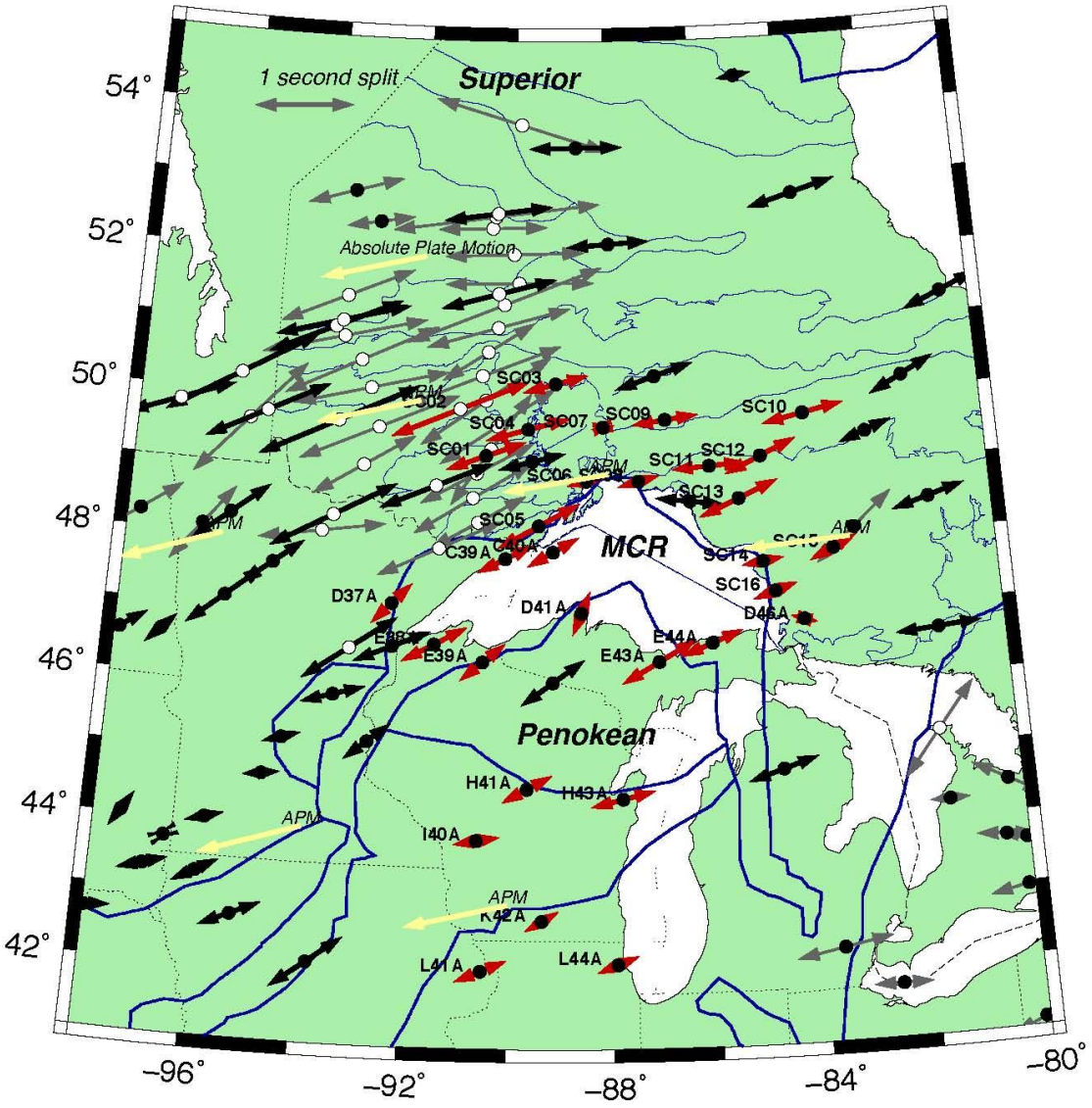

Figure 6.1: shear wave splitting results. The length of the arrow is the split time while the direction of the arrow is the orientation of fast shear wave. The split time of 1.1 s or more are

dotted white. The grey arrows show published splitting results (Silver and Kaneshima, 1993, Barruol et al., 1997, Kay et al., 1999**,** Fouch et al., 2000) obtained using various methods while the red arrows show results from this study and black arrows show results from published studies (Frederiksen et al., 2007, Frederiksen et al., 2013b) using the same method as this study. The yellow arrows show the direction of the absolute plate motion (see text for details). Thick solid blue lines indicate tectonic boundaries from Whitmeyer and Karlstrom (2007); thinner blue lines are Superior subdivisions within Ontario (Stott, 2011).

These observations form the basis of the discussion in subsequent subsections. The tectonic belt boundaries and APM directions allow me to relate them to my measurements. The APM direction was calculated for each point using MORVEL 2010 model. MORVEL is an acronym for Mid-Ocean Ridge Velocity. This model is a set of angular velocities that describes the motions of tectonic plates relative to a no-net-rotation reference frame (Argus et al., 2011). Because DeMets et al (2010) state that among the published estimates of geological plate motions, MORVEL is the most self-consistent and complete, I selected it for this project.

6.1 Fast direction measurements

The fast direction, the orientation of the fast shear wave (ϕ), is represented on the map by the direction of the arrows. For the stations in this study, the fast direction ranges from 36° to 107° with an average error of +/- 16° (Table 6.1). The lowest direction of 36° was obtained from station D41A while the highest direction of 107° was obtained from station D46A. Both are Transportable Array stations located close to the Mid-Continent Rift axis along the same plane and exhibit very low split times (and correspondingly high fast-direction uncertainties). The

mean value for the fast direction is 69°. A NE-SW direction is common across the region except for station D46A, which has a SE-NW fast direction but tiny split, approximately zero.

The fast direction contour map shown in figure 6.2 gives a clearer image of spatial variations in this parameter. I noticed a gentle variation of the fast direction across the region. The fast direction ranges from 60 – 80° across most of the map, with isolated outliers, a region of lower values at the western edge, and a patch of higher values near the southern limit of the eastern edge. There is also a decrease in fast direction just south of the MCR (south of Lake Superior). An example of an outlier is at station D46A, which has a fast direction of 107°. However, D46A shows a null result (the split time error is greater than the observed split time) and so the fast direction obtained here may not be meaningful, particularly given how much it differs from adjacent stations.

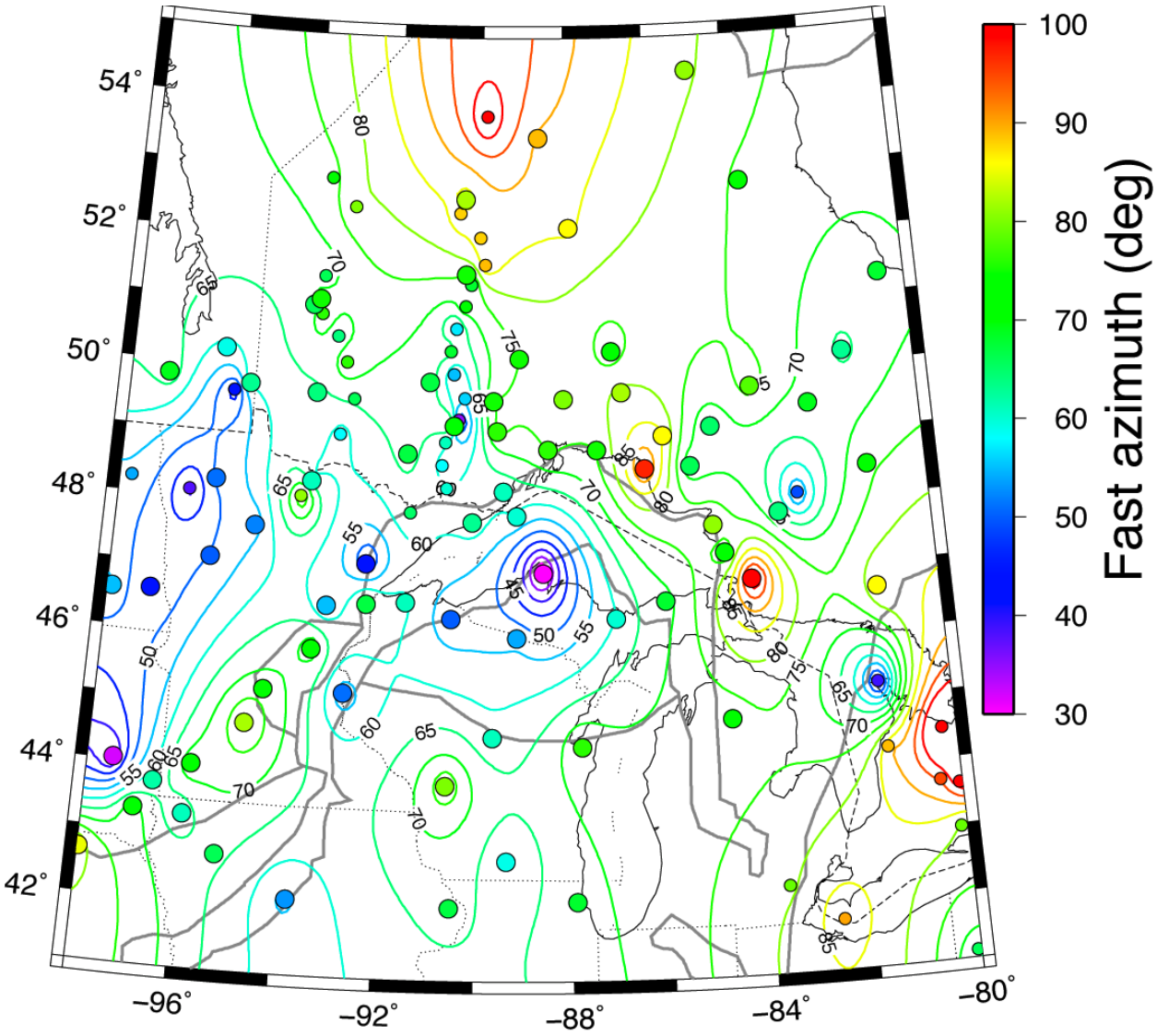

Figure 6.2: fast direction contour map. The contour interval is 5°. Large circles are this study and studies using the same methodology; small circles are other published studies.

6.2 Split time measurements

Generally, the split time results range from 0.25 s to about 1.48 s (Table 6.1). I detected near null measurements at SPREE station SC07 in the Nipigon Embayment and Transportable Array stations D46A and K42A. These are similar to the null measurements obtained in the Minnesota River Valley Terrane from a previous study (Frederiksen et al., 2013). Although my results show

a wide range of values for the split time measurements, most values fall below 1 s. The average value is about 0.60 s with an average error of around +/- 0.25 s.

The splitting map (figure 6.1) and split time contour map (figure 6.6) exhibit large spatially coherent variations across the study area. One major feature is the high split region (mostly above 1.1 s) in the western Superior Province. The high-split region is truncated by lower splitting regions to the south and east. The eastward truncation is sharp and abrupt while to the south the split times decrease more gradually.

The large split of more than 1.1 s in the western Superior decreases slightly to an average of 0.84 s at stations SC01, SC03 and SC04 just to the east. This reduction in the split time extends to the Nipigon Embayment in the east.

Figures 6.3 to 6.8 show histograms of the stations in different regions of my study area. The low split time zone east of Lake Superior has the lowest average split time of 0.36 s (figure 6.5) followed closely by the Nipigon Embayment region with an average split time of 0.38 s (figure 6.3). The Penokean, Yavapai and Mazatzal regions also have low split times with an average split time of 0.45 s. The MCR has low to moderate split time, while the WSP has high split times. The eastern Superior Province shows a moderate split with an average split time of 0.83 s.

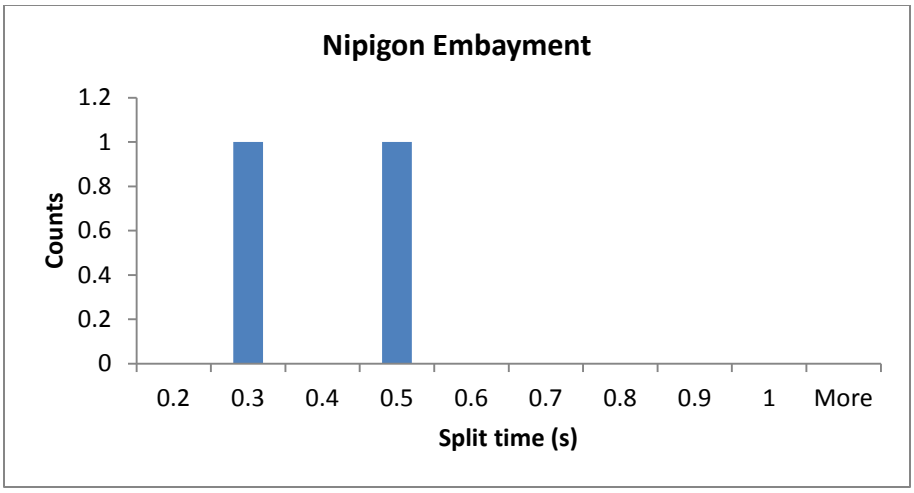

Figure 6.3: Histogram showing the split time of stations within the Nipigon Embayment. The average split time of stations is 0.38 s.

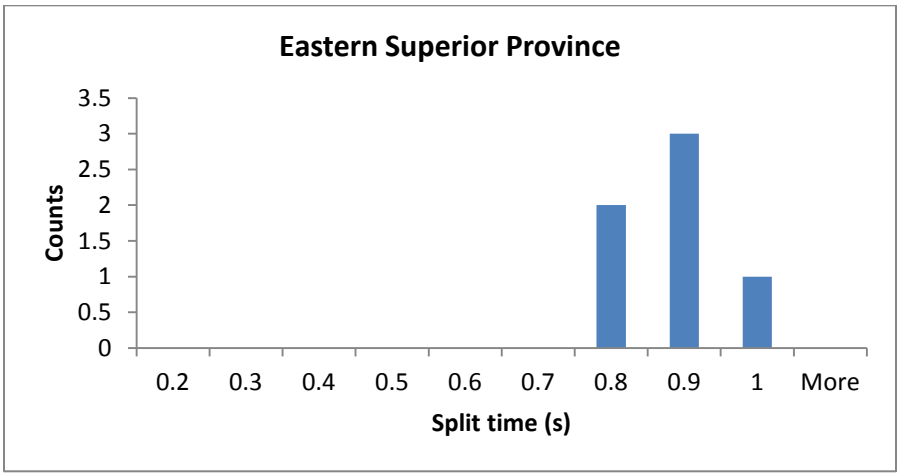

Figure 6.4: Histogram showing the split time of stations in the Eastern Superior Province. The average split time of the stations is 0.83 s.

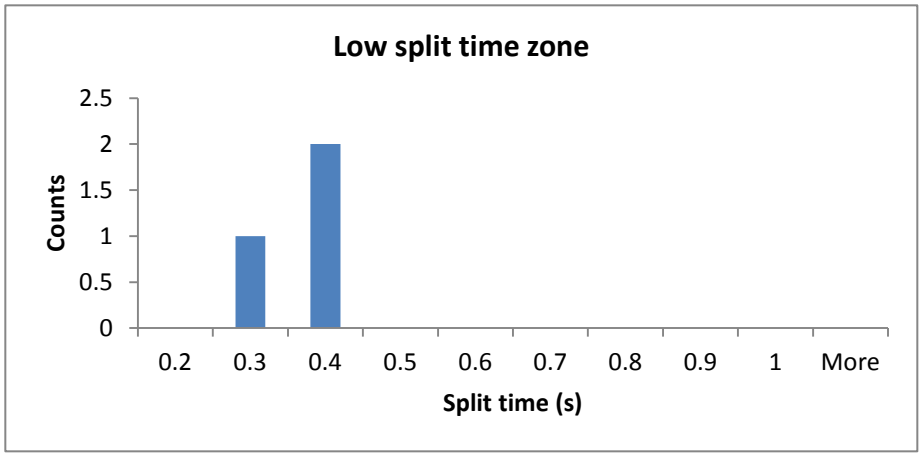

Figure 6.5: Histogram showing the split time of stations in the low split time zone. The average split time of the stations is 0.36 s.

Station SC07 just within the Nipigon Embayment shows a near null measurement of split time (0.25 s). The difference between the split time measurements obtained from stations on both sides of the Nipigon Embayment is about 0.6 s. This change represents a very large difference within a short distance. Stations SC06 and SC08 located south of the Nipigon Embayment, but along the rift axis, also show smaller split times of 0.43 s and 0.45 s respectively.

In addition, there is a glaring split time change to the southwest of the western Superior Province. The high split in the western Superior is abruptly truncated to the south. This observation is more noticeable in the split time contour map (figure 6.6). The southern part of the western Superior, investigated in previous studies (e.g, Frederiksen et al., 2013) and shown in figure 6.1, shows a low split time. Although stations in this current investigation do not cut through this region, it is obvious that there is sharp split time change between this region and the western Superior.

I noticed a trend of low split time along the arms of the MCR and around Lake Superior where the two arms meet. Results from 14 stations (SC05, SC06, SC08, SC14, SC16, C39A, C40A, D37A, D41A, D46A, E38A, E39A, E43A, and E44A) close to the arms of the MCR reveal an average split time of about 0.54 s (figure 6.6). Excluding stations SC05, E38A and E43A that have comparatively high split times of 0.85, 0.78 and 0.88 s respectively, the average split time of stations along the rift axis is as low as 0.46 s (figure 6.7). This result shows that the rift axis is a low split time region. Stations H41A, H43A, I40A, K42A, L41A and L44A in the Penokean, Yavapai and Mazatzal Provinces south of the MCR also show a consistently low split time of about 0.45 s on the average (figure 6.8), with a near null measurement of 0.25 s at station K42A. All these stations are in fairly close proximity to the null measurement found to their west around the Minnesota River Valley Terrane.

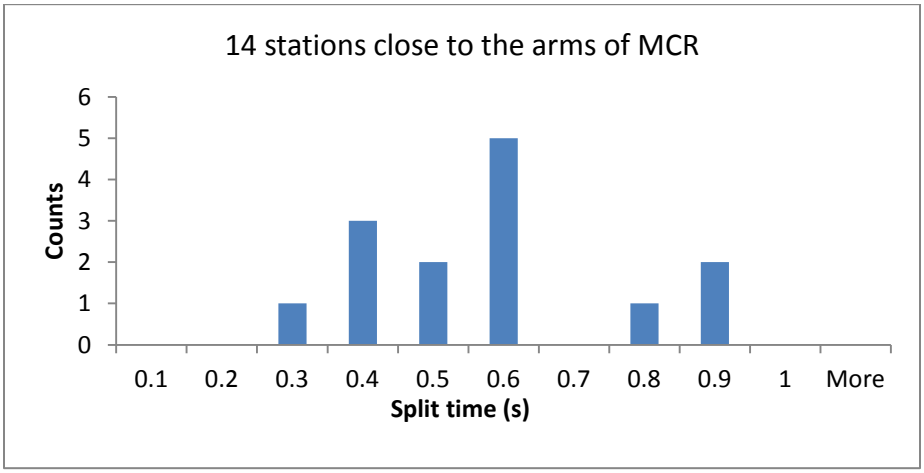

Figure 6.6: Histogram showing the split time of stations SC05, SC06, SC08, SC14, SC16, C39A, C40A, D37A, D41A, D46A, E38A, E39A, E43A, and E44A, close to the arms of the MCR. The average split time of the stations is 0.54 s.

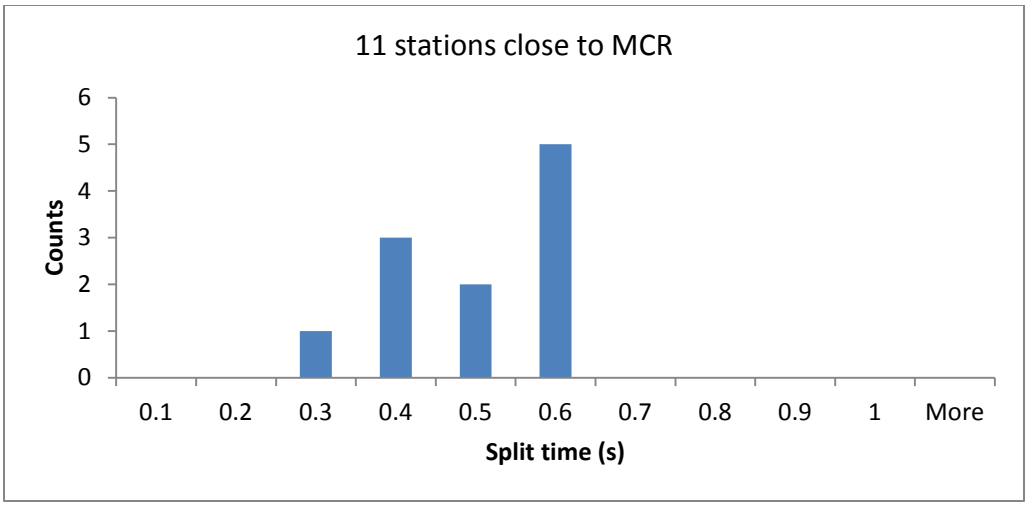

Figure 6.7: Histogram showing the split time of 11 stations (SC06, SC08, SC14, SC16, C39A, C40A, D37A, D41A, D46A, E39A, and E44A) close to the arms of the MCR. The average split time is 0.46 s.

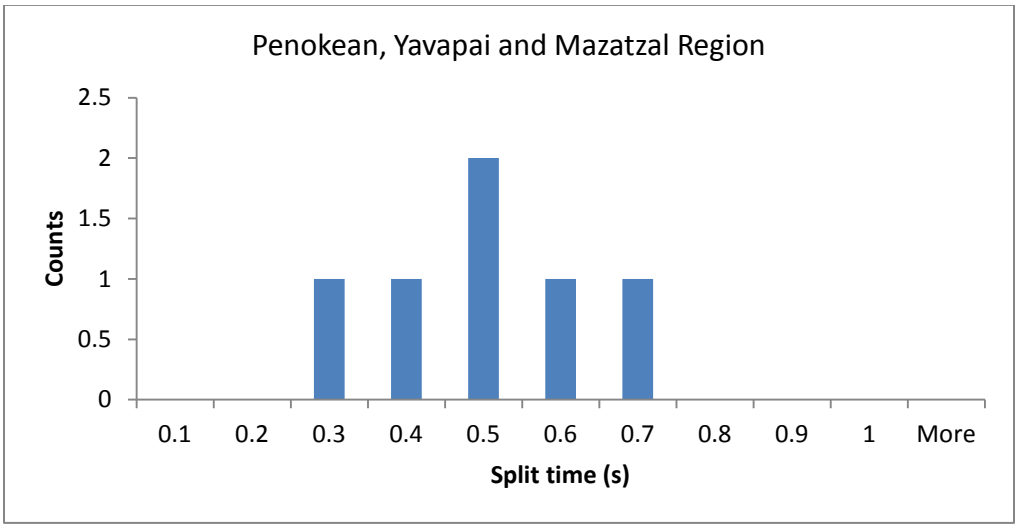

Figure 6.8: Histogram of stations H41A, H43A, I40A, K42A, L41A and L44A in the Penokean, Yavapai and Mazatzal Provinces. The average split time is 0.45 s.

The split time contour map gives a clearer image of the variation of the split time across the whole map region (figure 6.9). The colour coding makes it easier to interpret than the split time

map (figure 6.1). The sharp significant anisotropic boundary found to the east of the western Superior Province is clearer. The low anisotropy beneath the Nipigon Embayment is also evident in the split time contour map. Moreover, looking closely into figure 6.6, the truncation of the high split south of the WSP is becomes more obvious. Another noticeable observation on this contour map is the generally low split time around the rift axis and in the six stations within the Penokean, Yavapai and Mazatzal Provinces.

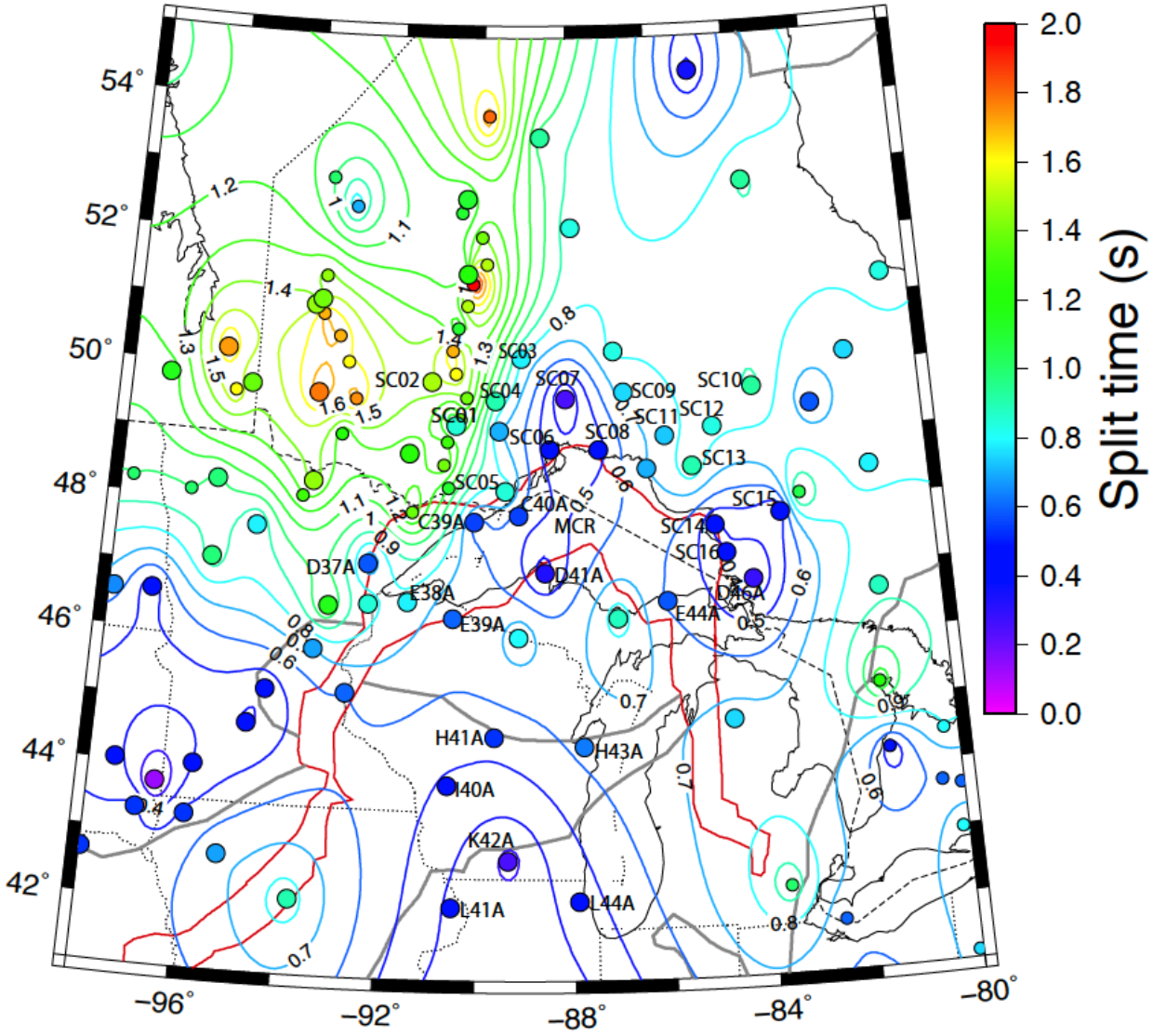

Figure 6.9: split time contour map. The contour interval is 0.1 s.

We will make a connection between these results, the geology of our study region and the MCR in the next chapter.

CHAPTER SEVEN

INTERPRETATION

7.0. Introduction

Splitting parameter (ϕ and δt) results help us to understand the anisotropic properties and fabric beneath a particular seismic station and are usually related to the tectonic environment beneath a station. The fast direction, ϕ, usually indicates the direction of the dominant upper mantle fabric beneath a station, assuming that the splitting results from aligned olivine crystals, and that the crustal contribution is minor. It also generally corresponds to the direction of maximum shear beneath a station. On the other hand, the split time, δt, refers to the total effective fabric beneath a seismic station (Frederiksen et al., 2007). Due to the lack of depth resolution in most shear wave splitting measurements (Long and Silver, 2009), I will not base judgements or inferences on precise depths. The shear wave splitting parameter results will help us understand the direction of the dominant mantle flow, the extent of upper mantle anisotropy in these regions, and the variation of the lithospheric fabric across the region.

I will use my results from Chapter Six to discuss and understand the effect of the Mid-Continent Rift on the lithospheric fabric within and around the Superior Province. I will be interpreting the geology of the Mid-Continent Rift based on our results and relating it to previous work on this region. Furthermore, I will show how my results relate to results of other geophysical studies such as tomography.

7.1. Depth of Anisotropy

7.1.1. Single layer

The shear wave splitting method used in this work distinguishes between single-layered anisotropy and more complex scenarios, given sufficient data. Generally, a single-layer model is adequate to explain my SKS data set, as explained below.

A splitting error surface indicates which values of the shear wave splitting parameter are compatible with the data set used to estimate it. The error surface is usually the same for all events with the same incident polarization. Figure 7.1 shows stacks of error surfaces for all events in each of a series of 10° wide polarization swaths at a typical station. The white star at all stations is the final shear wave splitting parameter (ϕ, δt) pair chosen for that station. The white star appears in a low-error (black) region for all the swaths, indicating that the single layer solution it represents is compatible with the entire data set.

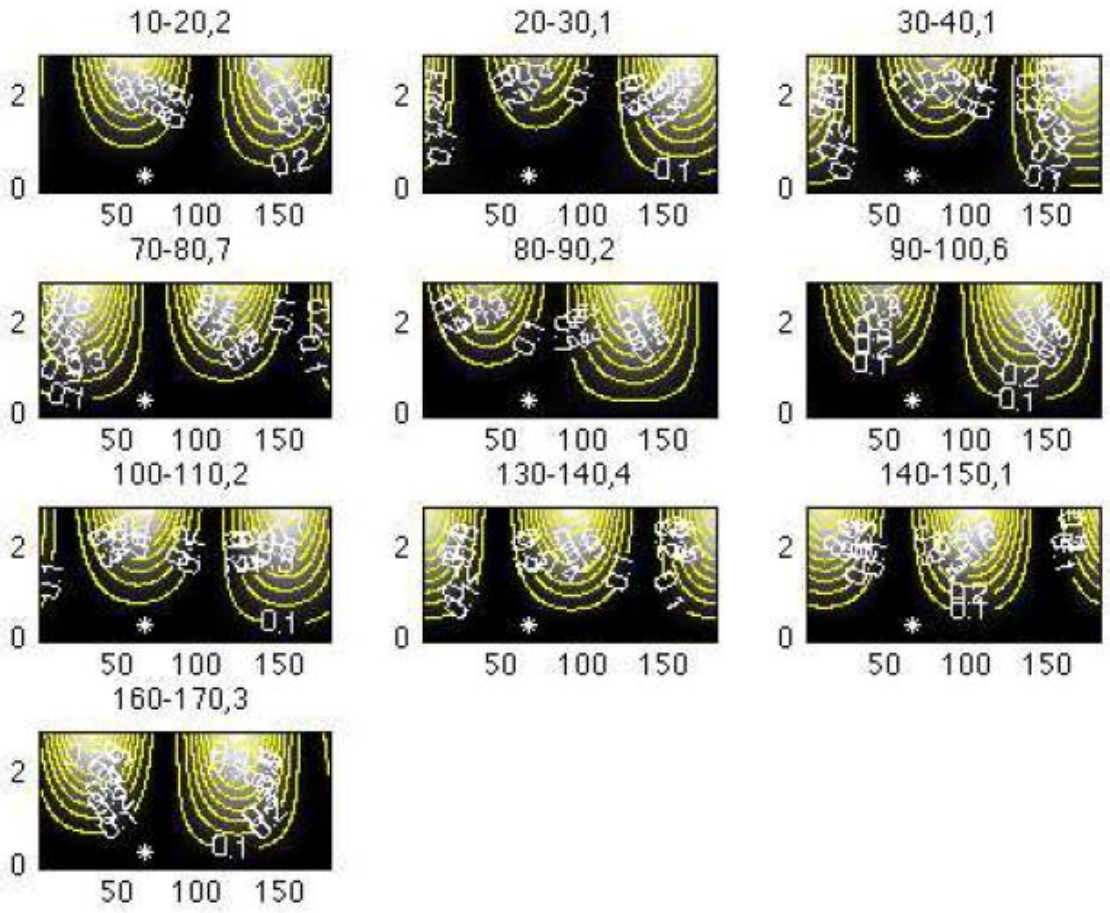

Figure 7.1: Shear wave stacking results showing different polarization swaths for station L41A. The label indicates the swath range (e.g. 30° - 40°) and the number of events in that swath.

Though all stations in my data set are compatible with a single-layer model according to this criterion, I cannot entirely rule out the presence of multiple layers of anisotropy; I can, however, state that the data set does not require multiple layers.

7.1.2 Asthenosphere or Lithosphere

Crustal anisotropy, which is a potential contaminant in a shear wave splitting signal, produces a typical delay time value of ~0.1 – 0.2 s (Long and Silver, 2009). Confirming this value using the Superior crustal structure observed by Musacchio et al., (2004) paper, using perpendicular

refraction lines, I considered the anisotropic layer they detected in the lower crust just above the Moho. The observed velocities of this layer,

$V_{fast} = 7.5\ kms^{-1}$, $V_{slow} = 6.9\ kms^{-1}$, $V_{average} = 7.2\ kms^{-1}$

yield an anisotropy of 8.3 %

The thickness, z of this layer is approximately 10 km and assuming a V_p/V_s of 1.6, the velocities of the S-wave would be

$V_{fast} = 4.7\ kms^{-1}$, $V_{slow} = 4.3\ kms^{-1}$

giving a split time,

$\delta t = z/V_{slow} - z/V_{fast} \approx 0.2$ s

The delay times measured in this study are far greater than this value, except for the null/near-null measurements recorded, which are also low but still greater than 0.2 s. Although there is some evidence of crustal anisotropy in my study area in previous studies, crustal fabrics are not generally strong or coherent in the Superior Province (Musacchio et al., 2004). This implies that the crust is likely not a major source of anisotropy in this region.

Correlation between fast direction and major tectonic belt boundaries usually implies lithospheric anisotropy, while correlation with the absolute plate motion directions suggests asthenospheric anisotropy (Frederiksen et al., 2006). The fast directions observed in this study in the western Superior Province are generally close to both tectonic belt boundaries and absolute plate motion direction, and so are compatible with both lithospheric and asthenospheric sources (figure 6.1). However, the large split time variation observed over the study area is difficult to explain using asthenospheric mechanisms. This is because asthenospheric variations are mantle flow variations, and the mantle flow pattern is probably fairly uniform given the consistent APM direction and plate velocity. Therefore, lithospheric anisotropy is more probable.

Another indication of lithospheric anisotropy is the sharp change in the fast direction and the reduction in the split time around station D37A at the boundary between the WSP and the MCR. This change in direction occurs over a distance of about 100 km. The ray length for SKS in this region was calculated using the Tau-P toolkit (Crotwell et al., 1999). Assuming an approximate ray length of 11,000 km, a depth of 250 km (around the base of the lithosphere), a frequency of 0.2 Hz, an S velocity of about 4.5 km/s (upper mantle), and so a wavelength of 4.5/0.2=22.5 km, the Fresnel zone width will be about 106 km. Two stations less than 106 km apart should have overlapping Fresnel zones at the base of the lithosphere and below. Overlapping Fresnel zones will cause surface measurements to vary smoothly, even when the underlying structure changes sharply, so sharp changes in measurements indicate shallower structure. Many strong changes occur between closely spaced seismic stations in this study, making it probable that much of the observed anisotropy in my results is located in the lithosphere and not the asthenosphere.

The lithospheric thickness in the central and western Superior Province varies between approximately 140 and 250 km (e.g., Darbyshire et al., 2007; Van der Lee and Frederiksen, 2005). The presence of thick lithosphere in the western Superior, coupled with the fact that anisotropy in this region cannot be deeper than 410 km (due to loss of olivine via phase transition) makes lithospheric anisotropy dominance in this region probable, given that the thick lithosphere in this region implies less asthenosphere above the 410 discontinuity. I believe that most of the anisotropy is likely to be in the lithosphere rather than the asthenosphere. Given the Fresnel-zone argument above, the major source of lateral variations is probably lithospheric, even if an asthenospheric component is present. Thus, interpretation in this study will primarily be in terms of the lithosphere.

7.2 Correlation of the splitting result with seismic velocity

There are distinct similarities between my result and P-wave tomography (Frederiksen et al., 2007 and 2013a). The high velocity (Frederiksen et al., 2013b) (figure 7.2), Western Superior Mantle Anomaly (WSMA), coincides with my strong splitting zone in the same region.

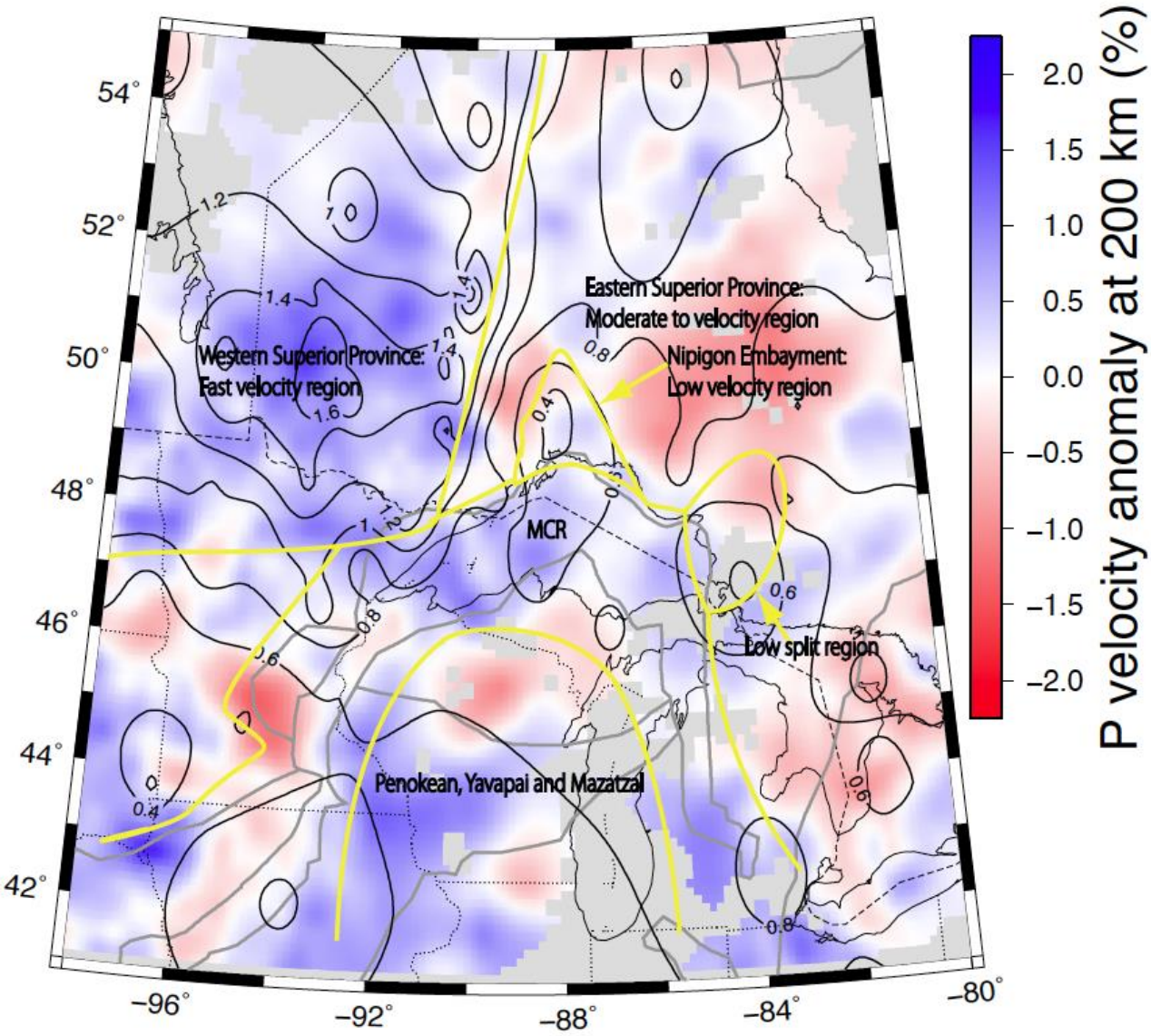

Figure 7.2: Tomography result showing a low P velocity anomaly beneath the Nipigon Embayment and high velocity anomaly in the western Superior Province. Black contours are split time (this study); colour background is P velocity from Frederiksen et al. (2013a)

Another notable correlation exists in the Nipigon Embayment, where a low velocity anomaly coincides with the very low split time observed in this study. There is no obvious correlation between the split time and velocity elsewhere in the study region. There is generally high

velocity and low split time in the southwest corner of the map, while much of the rest of the map is low velocity and shows moderate split time.

7.3 Zones of lithospheric anisotropy

My results show lateral anisotropy variations, which I attribute to lateral heterogeneity in lithospheric anisotropy. The major zones of anisotropy in this study are shown in figures 7.3 and 7.4. In the next subsections, I interpret the lithospheric features in the regions indicated.

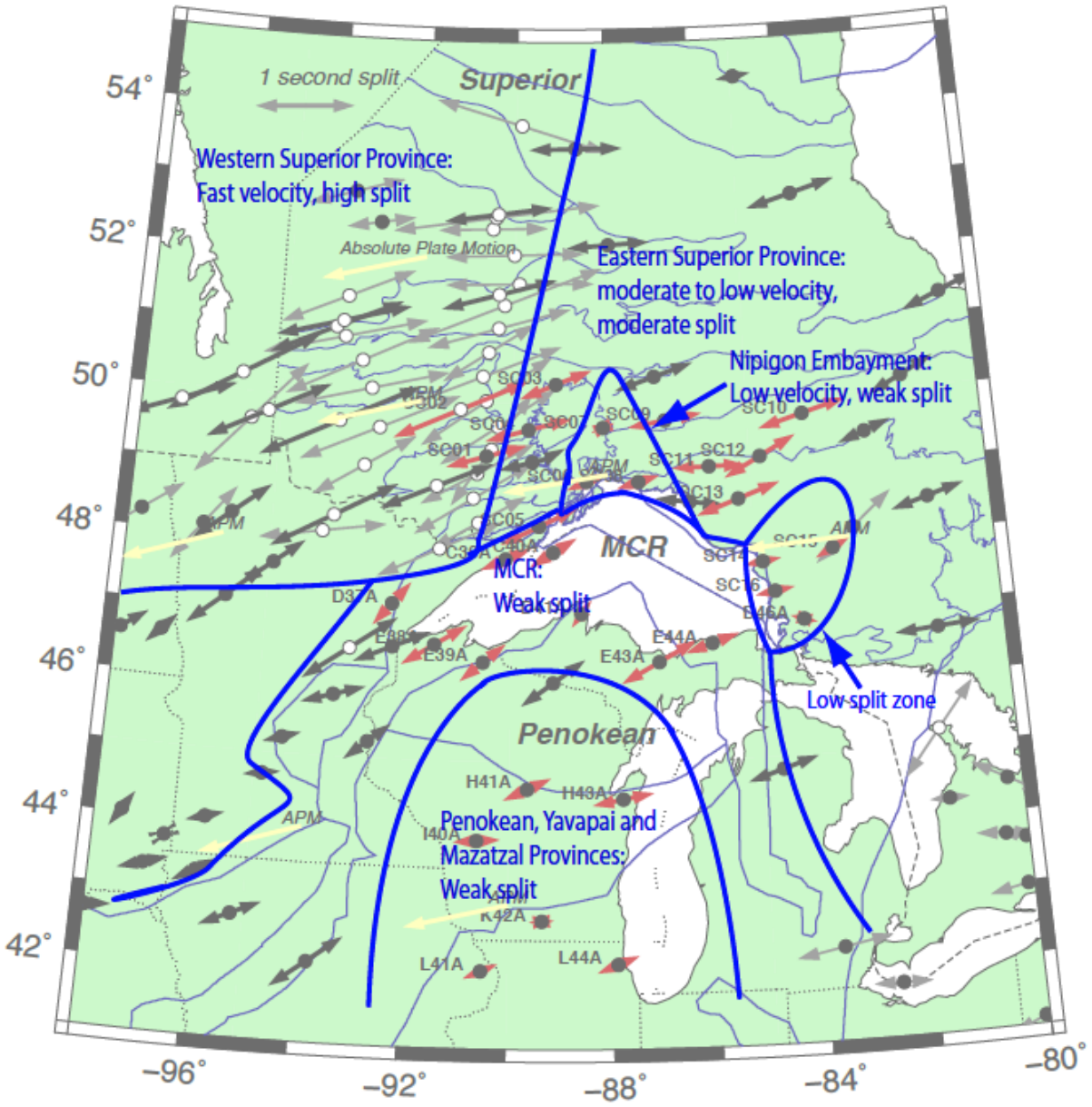

Figure 7.3: Major zones of lithospheric anisotropy determined in this study, superimposed on the shear-wave splitting map from figure 6.1.

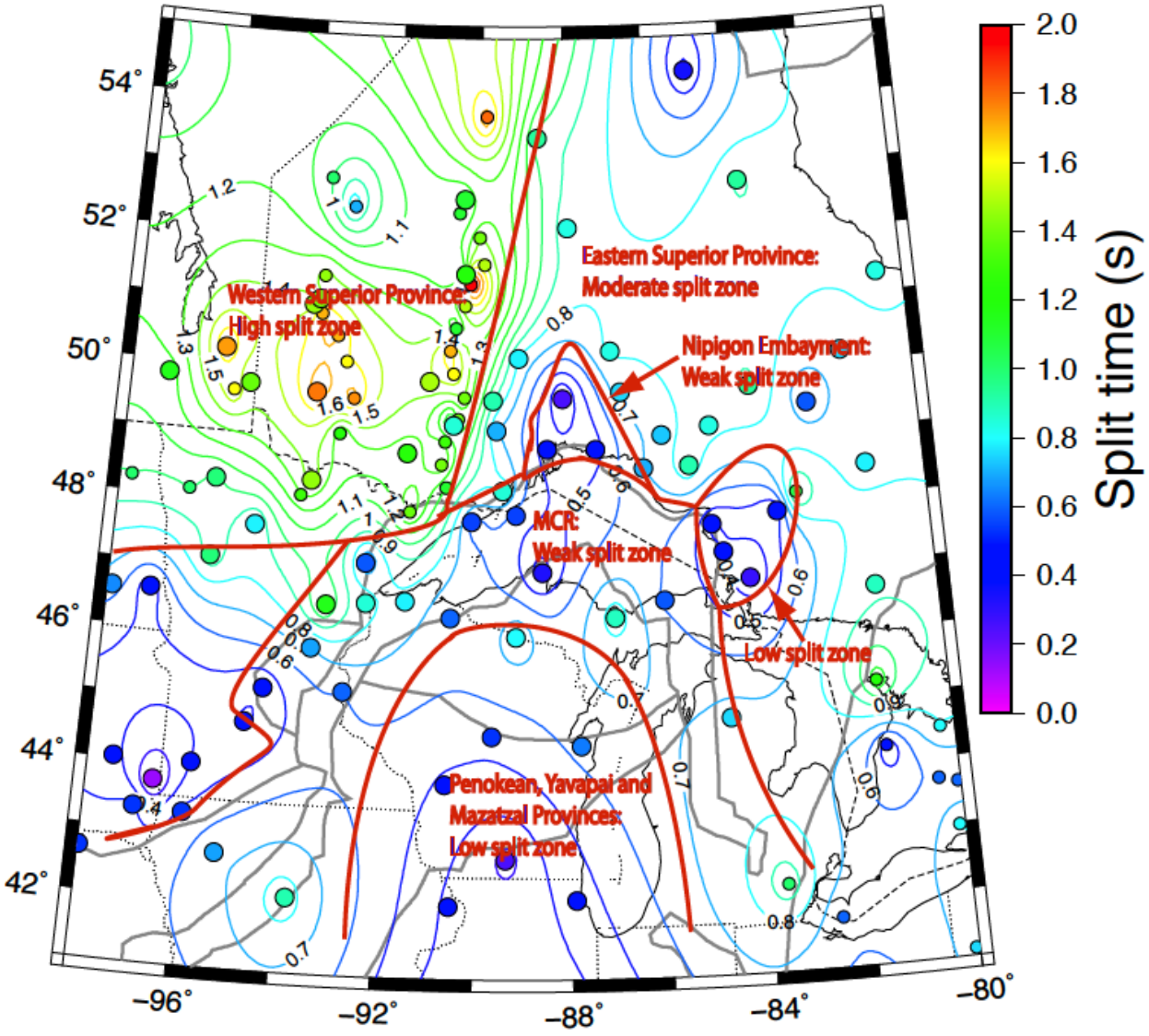

Figure 7.4: Shear wave split time contour map showing major zones of lithospheric anisotropy, superimposed on the split time contour map from figure 6.3.

7.3.1 Western Superior

The upper mantle of the western Superior differs significantly from neighbouring regions. The western Superior Province has a high P velocity and a consistent ENE fast direction and a split time mostly >1 s.

Previous studies such as LITHOPROBE (Kay et al., 1999) and the APT89 experiment (Silver and Kaneshima, 1993) observed moderate to large δt values (1.1 – 2.1 s) with a direction of fast polarization that generally aligns with the strike of the regional geologic boundaries over a large region of the western Superior Province. This is in agreement with my results in the western Superior Province, where we observed a concentration of split times of 1.1 s and above. My splitting results are also consistent with Rayleigh-wave modelling by Darbyshire et al., (2007) which indicated strong lithospheric anisotropy in the western Superior with a possibility of a WSW-ENE fast direction.

There is a good correlation between high velocities (Frederiksen et al, 2007) in the study area and large SKS split times. The transition from strong split to weaker split observed around 91°W longitude of the western Superior Province is similar to the transition from positive P velocity anomaly to negative P velocity anomaly observed in the same region in tomography results (Frederiksen et al., 2007). The boundary of the abrupt split time change observed around 91°W longitude indicates a sharp change in the anisotropy of the study area and demarcates the boundary between a thick lithospheric fabric in the WSP and what I interpret to be a reset lithosphere in the Nipigon Embayment, as noted below.

The large split time observed in the western Superior Province may be an indication of thick lithosphere or enhanced lithospheric anisotropy. Due to the large thickness (200 – 250 km) of lithosphere beneath this part of the Canadian Shield, it is likely that lithospheric anisotropy, representing "frozen" remnants of past deformation, is responsible for the observed splitting (Frederiksen et al., 2013) in this region. The high velocity peculiar to the western Superior Province is possibly a consequence of the alignment of remnant slabs related to the accretion of the Superior Province and may possibly be as a result of closer spacing of sutures compared to

elsewhere in the Superior (Frederiksen et al., 2007). The lithospheric fabric in the western Superior shows no evidence of having been altered by later tectonic events.

7.3.2 Eastern Superior

My splitting results for the eastern portion of the Superior Province show a moderate anisotropy. The moderate split time in this region is 0.73 – 0.93 s, and less than in the WSP. Frederiksen et al., (2006) recorded a weaker split with an average value of 0.66 s in this region. There is generally an ENE-WSW direction of the fast shear wave, similar to what is detected in Rondenay et al., (2000a,b), around the eastern Superior Province. This direction aligns with the tectonic boundaries and the APM.

Little variation is observed in the splitting results within the eastern Superior region except for the Nipigon Embayment (discussed separately) and a zone of very weak splits at stations SC14, SC15, SC16 and D46A east of Lake Superior. This low split zone (figures 7.3 and 7.4) may be related to the Nipigon Embayment just west, though it does not correspond to a velocity anomaly or a known geological feature. This is possibly a similar feature to the Nipigon Embayment and may also have taken part in the rifting process.

The LITHOPROBE AG transect experiment (Rondenay et al., 2000a,b) and a separate tomography study using POLARIS data (Aktas and Eaton, 2006) both detected a linear low-velocity anomaly in the eastern Superior Province, which is surrounded by regions with velocities higher than average that may be related to a thick lithospheric root (Darbyshire et al., 2007). This low-velocity feature is attributed to the Great Meteor hotspot track (Frederiksen et al., 2006), which is relatively young, 115–140 Ma (Eaton and Frederiksen, 2007), and a result of plate motion over a fixed or slow-moving hotspot (Frederiksen et al., 2007). Darbyshire et al.

(2007), reported that northeastern Ontario (referred to as the eastern Superior in this study) can be characterized by a thick lithosphere ranging from about 200 km to 240 km and a low-velocity zone at depths greater than 250 km. It is also believed that the shape of the thick Superior cratonic keel may have had a considerable influence on the hot plume material, making it deflect towards regions of thinner lithosphere (Darbyshire et al., 2007). Mantle plumes have played a major part in the modification of lithospheric root in many parts of the Superior (Darbyshire et al., 2007). Therefore, I interpret the moderate split times in the eastern Superior to be the result of Great Meteor hotspot activity modifying the lithosphere and weakening the anisotropy.

7.3.3 Nipigon Embayment

Tomography results such as Frederiksen et al. (2007) suggest that an anomalous structure is present north of Lake Superior. This low-velocity anomaly lies within the crustal bounds of the Nipigon Embayment. Perry et al. (2004) interpreted the Nipigon velocity anomaly as a relic of the ancient upwelling which fed the Nipigon magmas. The Nipigon Embayment shows a magnetotelluric response contrast to those in the surrounding Superior Province, suggesting the resistivity of the whole crust, and the underlying mantle were affected by Proterozoic tectonic processes (Ferguson et al., 2005). My results show that there is a null or very low value of split time (0.25 – 0.45 s) in the Nipigon Embayment, which is different to what we see in other parts of the Superior Province, and among the lowest splits measured in my study area.

The very weak splits within the Nipigon Embayment feature indicate that the lithospheric fabric within this region is essentially gone. This might be due to removal of the fabric through erosion of the lithosphere and its replacement with new material, or modification of the lithosphere that eliminated the fabric. The Nipigon Embayment may be a fossil hotspot feature in which a heat

source below cut through the entire lithosphere. This upwelling process might have led to the generation of the mafic and ultramafic intrusions associated with the Nipigon Embayment. It is useful to note that the Nipigon Embayment was formed before the MCR (Hollings et al., 2007), and that the diabase sills and intrusions around Lake Nipigon are the oldest expression of igneous activity associated with the MCR (Hearnan et al., 2007), which implies that the magmatic activities in this region might have predated the rift and perhaps led to its initiation.

Another observable inference in the Nipigon Embayment is that the direction of the fast shear wave remains parallel to the tectonic belt boundaries and absolute plate motion and is mostly nearly NNE-SSW like its surroundings. This suggests that either the fabric was weakened, but not completely eliminated, by thermal activity, or that the remaining splitting is asthenospheric or crustal.

The presence of sills rather than dykes (common in many failed rifts) indicates that the Nipigon Embayment was not extensional during the rifting event. In rift environments, dykes do not always reach the surface; however with the erosional state of the Nipigon embayment, some dykes should have been exposed if present (Hart and MacDonald, 2007). Therefore, the Nipigon Embayment is probably not a failed arm of the MCR. Hart and MacDonald, (2007) also suggest that the structures of the Embayment might have reacted to the rifting event, disallowing the formation of a rift arm, since they were formed prior to the Mid-Continent Rift.

7.3.4 Mid-Continent Rift

The fast directions of most stations within the MCR but adjacent to the WSP and Nipigon Embayment are parallel to the rift axis, which suggests alignment of LPO along the rift axis, but also aligns with the APM. However, stations south of Lake Superior, adjacent to the Penokean

Orogen, possess fast directions nearly perpendicular to the rift axis and not in the same direction as the APM. I also see considerable split time variation within the MCR. The results of this study show that the MCR is a relatively weak split zone (figures 7.3 and 7.4) with split times ranging from 0.33 s to 0.88 s. The split time in the MCR is not as low as in the Nipigon Embayment or the weak-split zone east of Lake Superior.

Seismic velocity appears fairly low in the MCR. However, the resolution by the tomography results of the MCR in previous studies such as Frederiksen et al. (2013a) is poor due to limited numbers of seismic stations around the MCR at that time. Data from SPREE seismic stations, through the ongoing tomography studies of Trevor Bollman (Northwestern University), will improve on the resolution of this region.

The relatively weak split around the MCR indicates that there is weaker anisotropy in this region and suggests the lithospheric fabric in this region has been thinned or modified. Although the split times within the rift axis are weak, they are more than the expected splitting for crustal anisotropy, therefore it is likely that at least some of the SKS splitting in the MCR occurs in the mantle.

The splitting results in this study shows that the fabric in the Nipigon Embayment is more extensively modified than in the MCR. This suggests that the Nipigon Embayment structures are deeper rooted, which is consistent with a hotspot mechanism. The Nipigon Embayment hotspot may have triggered the rifting events that were later driven by plate-tectonic forces (Merino et al., 2013). I observed that the MCR avoids high-split regions (east and west Superior), which suggests correlation between strong fabric and mechanical strength of the lithosphere. This might be the reason why rifting happened south of Nipigon Embayment and not to the west (western

Superior) or north/east (eastern Superior) of it. The observed splitting footprint of the MCR in this study (figure 7.3) is wider than the crustal MCR. My splitting result in this study shows a width extension of the known MCR footprint. This could possibly suggest that the lithospheric MCR is wider that the crustal feature.

There is a significant heat flow variation in my study region (figure 7.5). The range of heat flow in the MCR is low, 20 –31 mWm^{-2} (Hart et al., 1994) especially around the northwestern region of Lake Superior. There is a conspicuous change in heat flow along N-S line between 90° and 91°W (figure 7.5), which coincides with the region of sharp split time change between the western Superior and the Nipigon Embayment region of this study.

The low heat flow region in figure 7.5 coincides with the band of very high Bouguer gravity anomalies (Perry et al., 2004). The gravity anomaly seen in the MCR does not extend to the Nipigon Embayment indicating that the volume of the intrusives in the region is small. This implies that the Nipigon Embayment might have only led to the initiation of the MCR, and was not necessarily a driving force of the subsequent rifting process.

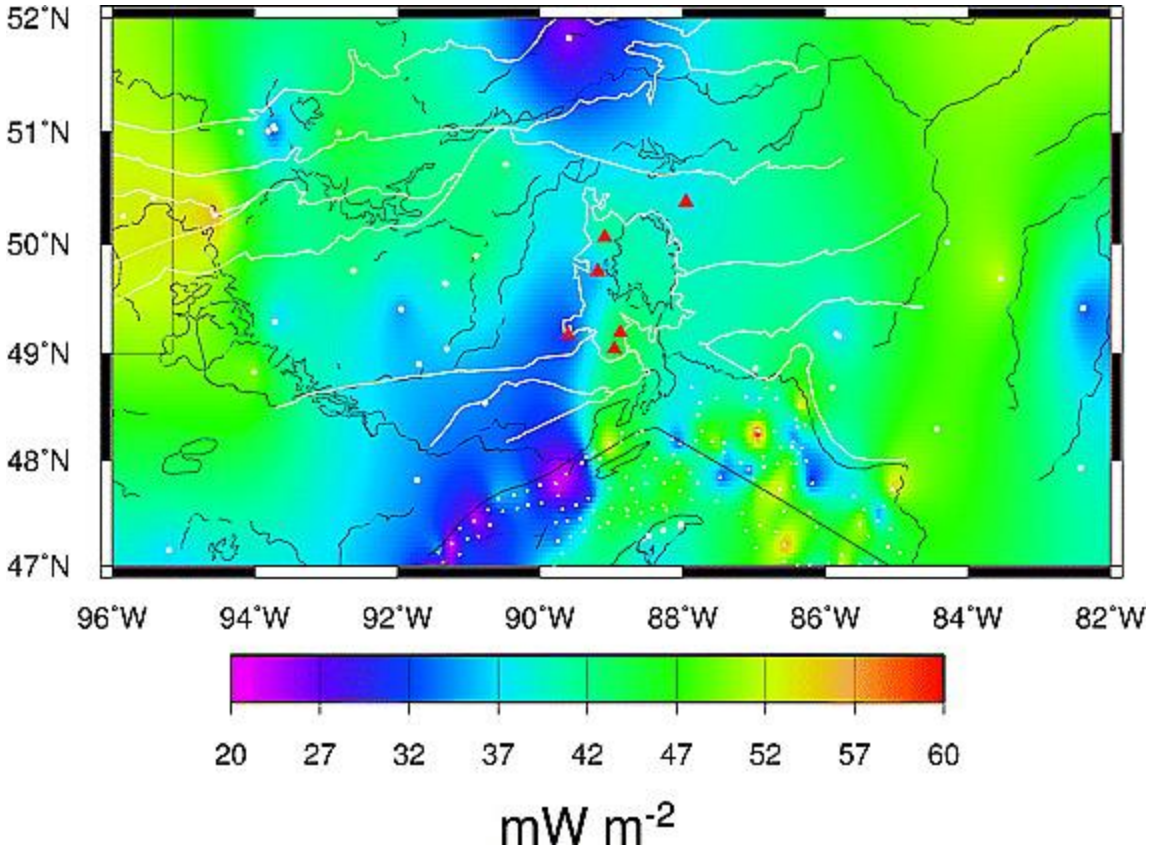

Figure 7.5: Heat flow map within our study region showing the western Superior, the Nipigon Embayment, the MCR and the eastern Superior Province (Perry et al., 2004)

7.3.5 Terranes south of Lake Superior region and the MCR

I observed low split times in the Penokean, Mazatzal and Yavapai provinces located in the south of the map region (figure 6.1). An average splitting time of 0.53 s was found. A split time of 0.25 s, which is the lowest in this study, is recorded at station K42A, located in this region. The fast direction generally aligns with the absolute plate motion direction but not particularly with the direction of tectonic boundaries in the region. This region is not well imaged by previous tomography results. The terranes in this region are younger than the MCR and zones north of it.

The Penokean, Yavapai and Mazatzal Provinces post-date Superior suturing events, and given the limited data in this study, I cannot distinguish the effect of rifting in these provinces.

CHAPTER 8

CONCLUSION AND RECOMMENDATIONS

8.1 Conclusion

I have analysed data from 31 seismic stations across the MCR around Lake Superior. 15 of these are Transportable Array stations while the remaining 16 are Canadian SPREE seismic stations. Using the shear wave splitting (Silver and Chan, 1991) transverse energy minimization and eigenvalue minimization methods, I have measured anisotropy, and thus lateral variations of lithospheric fabric across this region.

A single-layer model is sufficient to explain my data, although this does not necessarily imply that there is no more complex anisotropy.

The crust is likely not a major source of anisotropy in this region. Crustal fabrics are not strong or coherent in the Superior Province, and the observed split times are far greater than the typical crustal anisotropy delay time values of ~0.1 s - 0.2 s (Long and Silver, 2009). Most of the anisotropy resides in the lithosphere. I observed sharply changing anisotropy between closely spaced stations, also evidence of a lithospheric contribution.

Anisotropy and lithospheric fabric vary across the study area. My result shows high anisotropy in the western Superior Province, very low anisotropy in the Nipigon Embayment, low anisotropy in the MCR axis, and moderate to low anisotropy in the eastern Superior Province, with an isolated region of very low anisotropy east of Lake Superior. There is also low anisotropy in the Penokean, Yavapai and Mazatzal provinces.

There are correlations between seismic velocities obtained using tomographic methods and my shear wave splitting studies in the study region. Strong split times in the western Superior coincide with a high velocity region while weak splits in the Nipigon Embayment coincide with low velocity measurements in Frederiksen et al. (2007, 2013a). There are no obvious correlations in other regions on the study map.

This study confirms previous teleseismic studies (e.g. Frederiksen et al., 2007) and LITHOPROBE (Musacchio et al., 2004) studies that suggested that the western Superior Province is strongly anisotropic, with split times greater than 1.1 s. This is evidence that thick lithospheric fabric is present in this region. Furthermore, the fast direction observed in this region is consistent with both the direction of absolute plate motion and the direction of tectonic belt boundaries. The western Superior Province overlies an unusual lithospheric mantle with distinct strong anisotropy and high velocity. The strong lithospheric fabric in WSP is truncated to the south by the Mid-Continent Rift. The truncation of strong fabric to the east is also evidence of modification of the mantle fabric in this region.

Previous tomographic (Frederiksen et al., 2007, 2013) and magnetotelluric (Ferguson et al., 2005) studies reported an anomalous structure in the Nipigon Embayment. I observed a very low split (0.25 - 0.45 s), which indicates that the lithospheric fabric in this region may have been lost. I suggest that the Nipigon Embayment is a hotspot feature, which may have contributed to the initiation of the MCR rifting process.

The relatively weak split observed in the MCR suggests that the lithospheric fabric in this region might have been thinned or modified, though not as much as in the Nipigon Embayment. Thus, though the MCR may have been initiated by a hotspot below Nipigon Embayment through a

hotspot mechanism, this study suggests that it evolved by plate-boundary processes. The MCR avoids regions of high splits (east and west Superior) and occurred south of the Nipigon Embayment. This might suggest a correlation between mechanical strength of the lithosphere and strong fabric. My splitting results also suggest that the lithospheric MCR is probably wider than the crustal MCR due to the extension seen in the width of the MCR footprint especially around its arms.

A localized low split zone observed northeast of the MCR is a feature newly discovered by this study. It is similar in split time and extent to what I see in the Nipigon Embayment and may have also participated in the rifting process. The broader zone of moderate split times in the eastern Superior Province may be attributed to the Great Meteor hotspot track having modified the lithosphere and weakened its fabric.

This study has helped map the anisotropic extent and changes in the lithospheric fabric of my study area after the rifting process. The lithospheric fabric was most strongly modified in the Nipigon Embayment, the eastern Superior and in the MCR. These modifications might be due to different mechanisms, such as lithospheric thinning and hotspot modification. Smaller features such as my newly discovered low split zone to the east of Lake Superior may have also been involved in the rifting process.

8.2 Recommendations

1. Analyse more stations south of MCR and in the dense SPREE array along the MCR to see more detail of the effect of the MCR on the adjacent terranes.

2. Improve existing tomography and magnetotelluric studies of the study area using the Canadian SPREE seismic stations and further analysis of existing MT data.

3. Place ocean-bottom seismographs (OBS) in Lake Superior to extend this study into the Lake and see the extent of anisotropy and the strength of the fabric within the Lake Superior axis of the MCR.

References

Aktas K., D.W. Eaton, 2006. Upper-mantle velocity structure of the lower Great Lakes region. Tectonophysics, 420, 267–281

Allen, R.M. et al., 2002. Imaging the mantle beneath Iceland using integrated seismological techniques, J. Geophys. Res., 107, 2325, doi:10.1029/2001JB000595.

Anderson, J.L., 1983. Proterozoic anorogenic granite plutonism of North America, in Medaris, L.G., Byers, J.,Mickelson, C.W., and Shanks, W.C., eds., Proterozoic Geology: Selected Papers from an International Proterozoic Symposium: Boulder, Colorado, Geological Society of America Memoir 161, p. 133–154.

Ando, M., and Y. Ishikawa, 1982. Observations of shear-wave velocity polarization anisotropy beneath Honshu, Japan: Two masses with different polarization in the upper mantle, J. Phys. Earth, 30, 191-199.

Argus, D.F., R.G. Gordon, C. DeMets, 2011. Geologically current motion of 56 plates relative to the no-net-rotation reference frame. Geochemistry, Geophysics, Geosystems, 12, p. 11 http://dx.doi.org/10.1029/2011GC003751

Atekwana, E.A., 1996. A regional assessment of mapped geological and geophysical features of the Precambrian Basement within the Midcontinent Rift area, Geological Society of America Special Paper 308, 33-44.

Barruol, G., P. Silver, A. Vauchez, 1997. Seismic anisotropy in the eastern United States: Deep structure of a complex continental plate. J. Geophys. Res. 102, 8329–8348

Barth, A.P., J.L. Wooden, D.S. Coleman and C.M., Fanning, 2000. Geochronology of the Proterozoic basement of southwesternmost North America, and the origin and evolution of the Mojave crustal province Tectonics, v.19,616-629

Bickford, M.E., and B.M. Hill, 2007. Does the arc accretion model adequately explain the Paleoproterozoic evolution of southern Laurentia?: An expanded interpretation: Geology, v. 35, p. 167–170, doi:10.1130/ G23174A.1.

Bowman, J.R., M. Ando, 1987. Shear-wave splitting in the upper-mantle wedge above the Tonga subduction zone. Geophys J Roy Astr Soc 88:25–41

Butler, R., T. Lay, K. Creager, P. Earl, K. Fischer, J. Gaherty, G. Laske, B. Leith, J. Park, M. Ritzwoller, J. Tromp, L. Wen. 2004. The global seismographic network surpasses its design goal. Eos, Transactions, AGU, Volume 85, Issue 23, p. 225-229

Calais, E., M. Vergnolle, V. Sankov, A. Lukhnev, A. Miroshnitchenko, S. Amarjargal, and J. Deverchere, 2003. GPS measurements of crustal deformation in the Baikal-Mongolia area (1994

– 2002): Implications for current kinematics of Asia, J. Geophys. Res., 108(B10), 2501, doi:10.1029/2002JB002373.

Card, K.D., 1990. A review of the Superior Province of the Canadian Shield, a product of Archean accretion. Precambrian Research Volume 48, Issues 1–2, Pages 99–156

Card, K. D., and A. Ciesielski, 1986. DNAG no. 1. subdivisions of the Superior Province of the Canadian shield, Geosci. Can., 13, 5 – 13.

Chevrot, S., 2000. Multichannel analysis of shear wave splitting, J. geophys. Res., 105, 21 579–21 590.

Chevrot, S., 2006. Finite-frequency vectorial tomography: a new method for high-resolution imaging of upper mantle anisotropy. Geophysical Journal International, Volume 165, Issue 2, pages 641–657, DOI: 10.1111/j.1365-246X.2006.02982.x

Chevrot, S., N. Favier, & D. Komatitsch, 2004. Shear wave splitting in three-dimensional anisotropic media. Geophysical Journal International, Volume 159, Issue 2, pp. 711-720. GeoJI.159..711C

Clitheroe, G., and R. Van der Hilst, 1998. Complex Anisotropy in the Australian Lithosphere from Shear-wave Splitting in Broad-band SKS Records, Structure and Evolution of the Australian Continent Geodynamics, 26, pg 73 - 78

Condie, K.C., 1992. Proterozoic Crustal Evolution. Elsevier Science Publishers, 551.715-dc20 ISBN 0444887822

Crotwell, H.P., T.J. Owens, and J. Ritsema, 1999. The TauP Toolkit: Flexible seismic travel-time and ray-path utilities, Seismol. Res. Lett. 70, 154–160.

Darbyshire, F.A., D.W. Eaton, A.W. Frederiksen, and L. Ertolahti, 2007. New insights into the lithosphere beneath the Superior Province from Rayleigh wave dispersion and receiver function analysis, Geophys. J. Int., doi: 10.1111/j.1365-246X.2006.03259.x

DeMets, C., R.G. Gordon and D.F. Argus, 2010. Geologically current plate motions, Geophysical Journal International, v. 181, no. 1, p. 1-80, doi: 10.1111/j.1365-246X.2009.04491.x

DiCiccio, T.J., B. Efron, 1996. Bootstrap confidence intervals. Statistical Science 11: 189-228

Dickin, A.P., 2000. Crustal formation in the Grenville Province: Nd isotope evidence. Can. J. Earth Sci. 37, 165-181.

Eaton, D.W., and A.W. Frederiksen, 2007. Seismic evidence for convection-driven motion of the North American plate, Nature 446, 428–431, doi:10.1038/nature05675.

Ebinger, C.J., N.H. Sleep, 1998. Cenozoic magmatism throughout East Africa resulting from impact of a single plume: Nature, v. 395, p. 788–791, doi:10.1038/27417.

Efron, B. and R. Tibshirani, 1991. Statistical data analysis in the computer age, Science 253, 390-395.

Evans, M.S., J.M. Kendall, R.J. Wyllemann, 2006. Automated SKS splitting and uppermantle anisotropy beneath Canadian seismic stations. J. Geophys. Int. 165, 931–942.

Ferguson, I. J., J.A. Craven, R.D. Kurtz, D.E. Boerner, R.C. Bailey, X. Wu, M.R. Orellana, J. Spratt, G. Wennberg, M. Norton, 2005. Geoelectric response of Archean lithosphere in the western Superior Province, central Canada, Phys. Earth Planet. Inter., 150, 123–142.

Ferré, E.C., A. Gébelin, J.A. Conder, N. Christensen, J.D. Wood, and C. Teyssier, 2014. Seismic anisotropy of the Archean crust in the Minnesota River Valley, Superior Province, Geophys. Res. Lett., 41, doi:10.1002/2013GL059116.

Fischer, K.M., E.M. Parmentier, A.R. Stine, E.R. Wolf, 2000. Modeling anisotropy and plate-driven flow in the Tonga subduction zone back arc. J Geophys Res 105:16181–16191

Forsyth, D.W., 1975. The early structural evolution and anisotropy of the oceanic upper mantle, Geophys. J. R. Astron. Soc., 43, 103-162.

Fouch, M.J., K.M. Fischer, E.M. Parmentier, M.E. Wysession, and T.J. Clarke, 2000. Shear wave splitting, continental keels, and patterns of mantle flow, J. Geophys. Res., 105, 6255 – 6275

Franklin, J.M., W.H. McIlwaine, H.K. Poulsen, R.K. Wanless, 1980. Stratigraphy and depositional setting of the SibleyAnnual Reviews www.annualreviews.org/aronline Group, Thunder Bay district, Ontario, Canada. Can. J. Earth Sci. 17 : 633-51

Frederiksen, A.W., I.J. Ferguson, D. Eaton, S.K. Miong, and E. Gowan, 2006. Mantle fabric at multiple scales across an Archean-Proterozoic boundary, Eastern Ontario, Canada, Phys. Earth Planet. Inter., 158, 240–263.

Frederiksen, A.W., S.K. Miong, F.A. Darbyshire, D.W. Eaton, S. Rondenay, and S. Sol, 2007. Lithospheric variations across the Superior Province, Ontario, Canada: Evidence from tomography and shear wave splitting, J. Geophys. Res., 112, B07318, doi:10.1029/2006JB004861.

Frederiksen, A.W., T. Bollmann, F. Darbyshire, and S. Van der Lee, 2013a. Modification of continental lithosphere by tectonic processes: A tomographic image of central North America, J. Geophys. Res. Solid Earth, 118, 1051–1066, doi:10.1002/jgrb.50060.

Frederiksen, A.W., I. Deniset, O. Ola, and D. Toni, 2013b. Lithospheric fabric variations in central North America: Influence of rifting and Archean tectonic styles, Geophys. Res. Lett., 40, 4583–4587, doi:10.1002/grl.50879.

Godey, S., R. Snieder, A. Villasenor, and H.M. Benz, 2003. Surface wave tomography of North America and the Caribbean using global and regional broad-band networks: Phase velocity maps and limitations of ray theory, Geophys. J. Int., 152, 620–632

Hart, S.R., J.S. Steinhart and T.J. Smith, 1994. Terrestrial heat flow in Lake Superior.Canadian Journal of Earth Sciences, vol. 31, p. 698-708.

Hart, T.R. and C.A. MacDonald, 2007. Proterozoic and Archean geology of the Nipigon Embayment: implications for emplacement of the Mesoproterozoic Nipigon diabase sills and mafic to ultramafic intrusions. Can. J. Earth. Sci. 44: 1021–1040. doi:10.1139/E07-026

Heaman L.M., R.M. Easton, T.M. Hart, C.A. MacDonald, P. Hollings and M. Smyk, 2007. Further refinement to the timing of Mesoproterozoic magmatism, Lake Nipigon region, Ontario: Canadian Journal of Earth Sciences, v. 44, p. 1055–1086.

Hess, H. H., 1964. Seismic anisotropy of the uppermost mantle under oceans, Nature, 203, 629-631.

Hoffmann, P.F., 1988. United plates of America, the birth of a craton: early Proterozoic assembly and growth of Laurentia. Ann. Rev. Earth Planet. Sci., 16: 543-603.

Hoffman, P.F., 1990. Geological constraints on the origin of the mantle root beneath the Canadian Shield. Philosophical Transactions of the Royal Society of London, 331: 523-532.

Hollings, P., P. Fralick, and B. Cousens, 2007. Early history of the Midcontinent Rift inferred from geochemistry and sedimentology of the Mesoproterozoic Osler Group, northwestern Ontario: Canadian Journal of Earth Sciences, v. 44, p. 389–412, doi:10.1139/e06-084.

Holm, D.K., W.R. Van Schmus, L.C., Mac Neil, T.J. Boerboom, D. Schweitzer, and D. Schneider, 2005. U-Pb zircon geochronology of Paleoproterozoic plutons from the northern mid-continent, U.S.A.: Evidence for subduction flip and continued convergence after geon 18 Penokean orogenesis: Geological Society of America Bulletin, v. 117, p. 259-275.

Holm, D.K., R. Anderson, T.J. Boerboom, W.F. Cannon, V. Chandler, M. Jirsa, J. Miller, D.A. Schneider, K.J. Schulz, W.R. Van Schmus, 2007. Reinterpretation of Paleoproterozoic accretionary boundaries of the north-central United States based on a new aeromagnetic-geologic compilation. Precambrian Research 157, 71–79

Huismans, R. S., Y. Y. Podladchikov, and S. Cloetingh, 2001. Dynamic modeling of the transition from passive to active rifting, application to the Pannonian Basin, Tectonics, 20(6), 1021–1039, doi:10.1029/2001TC900010.

Karlstrom, K.E., and E.D. Humphreys, 1998. Influence of Proterozoic accretionary boundaries in the tectonicevolution of western North America: Interactionof cratonic grain and mantle modifications events:Rocky Mountain Geology, v. 33, p. 161–180.

Karlstrom, K.E., J.M. Amato, M.L. Williams, M. Heizler, C. Shaw, A. Read, and P. Bauer, 2004. Proterozoic tectonic evolution of the New Mexico region: A synthesis, in Mack, G.H., and Giles, K.A., eds., The Geology of New Mexico: A Geologic History: Albuquerque, New Mexico, New Mexico Geological Society Special Publication 11, p. 1–34

Kay, I., S. Sol, J.-M. Kendall, C. Thomson, D. White, I. Asudeh, B. Roberts, and D. Francis, 1999b. Shear wave splitting observation in the Archean Craton of western Superior, Geophys. Res. Lett., 26, 2669– 2672.

Kendall, J. M., S. Sol, C. J. Thomson, D. J. White, I. Asudeh, C. S. Snell and F. H. Sutherland, 2002. Seismic heterogeneity and anisotropy in the Western Superior Province, Canada: insights into the evolution of an Archaean craton. Geological Society, London, Special Publications, 199:27-44, doi:10.1144/GSL.SP.2002.199.01.02

Long, M. D., 2013. Constraints on subduction geodynamics from seismic anisotropy. Reviews of Geophysics, Volume 51, Issue 1, pages 76–112

Long, M. D., and P. G. Silver, 2009b. Shear wave splitting and mantle anisotropy: Measurements, interpretations, and new directions, Surv. Geophys., 30, 407–461.

Long, M. D. and T. W. Becker, 2010. Mantle dynamics and seismic anisotropy. Earth and Planetary Science Letters, Volume 297, Issues 3–4, 1, Pages 341–354

Magnani, M.B., K.C. Miller, A. Magnani, and K. Karlstrom, 2004. The Yavapai-Mazatzal boundary: A long lived assembly structure in the lithosphere of southwestern North America: Geological Society of America Bulle- tin, v. 116, p. 1137–1142, doi: 10.1130/B25414.1.

Matcham, I., 1997. Seismic anisotropy in the Wellington region from local events recorded at IRIS station SNZO, Honours dissertation, Victoria University of Wellington, Wellington, New Zealand.

Matcham, I., M.K. Savage, and K.R. Gledhill, 2000. Distribution of seismic anisotropy in the subduction zone beneath the Wellington region. New Zealand, Geophys, j. Int,. 140, 1 - 10

McLelland, J., J.S. Daly, J.M. McLelland, 1996. The Grevilla Orogenic Cycle (ca. 1350-1000 Ma) an Adirondack Perspective. Tectonophysics 265 (1996) 1 – 28.

Menke W., V. Levin, 2003. The cross-convolution method for interpreting SKS splitting observations, with application to one and two-layer anisotropic earth models, Geophys. J. Int., 154, 379–392.

Merino, M., G. R. Keller, S. Stein, and C. Stein, 2013. Variations in Mid-Continent Rift magma volumes consistent with microplate evolution. Geophysical Research Letters, Vol. 40, 1–4, doi:10.1002/grl.50295

Monteiller, V., and S. Chevrot, 2010. How to make robust splitting measurements for single-station analysis and three-dimensional imaging of seismic anisotropy, Geophys. J. Int., 182, 311–328.

Musacchio, G., D.J. White, I. Asudeh, and C.J. Thomson, 2004. Lithospheric structure and composition of the Archean western Superior Province from seismic refraction/wide-angle reflection and gravity modelling, J. Geophys. Res., 109, B03304, doi:10.1029/2003JB002427.

Ojakangas, R., G. Morey, and J. Green, 2001. The Mesoproterozoic Midcontinent Rift System, Lake Superior Region, USA, Sediment. Geol., 141, 421–442.

Percival, J.A., W. Bleeker, F.A. Cook, T. Rivers, G. Ross, and C.R., Van Staal, 2004. Panlithoprobe workshop IV: Intra-orogen correlations and comparative orogenic anatomy. Geoscience Canada, 31: 23-39.

Perry, H. K. C., C. Jaupart, J.C. Mareschal, F. Rolandone, G. Bienfait, 2004. Heat flow in the Nipigon arm of the Keweenawan rift, northwestern Ontario, Canada. Geophysical Research Letters, Vol. 31, L15607, doi:10.1029/2004GL020159

Restivo, A., G. Helffrich, 1999. Teleseismic shear wave splitting measurements in noisy environments Geophys. J. Int., 137 (3), pp. 821–830

Rino, S., Y. Kon, W. Sato, S. Maruyama, M. Santosh, D. Zhao, 2008. The Grenvillian and Pan-African orogens: world's largest orogenies through geologic time, and their implications on the origin of superplume. Gondwana Research, vol. 14, pp. 51–72

Rogers, J. J., and M. Santosh , 2004. Continents and supercontinents. Oxford University Press. QE 511.R59 551.136-dc22

Rondenay, S., M.G. Bostock, T. Hearn, D.J. White, H. Wu, G. Senechal, S. Ji, and M. Mareschal, 2000a. Teleseismic studies of the lithosphere below the Abitibi-Grenville Lithoprobe transect, Can. J. Earth Sci., 37, 415–426.

Rondenay, S., M.G. Bostock, T.M. Hearn, D.J. White, and R.M. Ellis, 2000b. Lithospheric assembly and modification of the SE Canadian Shield: Abitibi-Grenville Teleseismic Experiment, J. geophys. Res., 105, 13,735– 13,754.

Saltzer, R.L., J.B. Gaherty, T.H. Jordan, 2000. How are vertical shear wave splitting measurements affected by variations in the orientation of azimuthal anisotropy with depth? Geophys. J. Int., 141, pp. 374–390

Sandvol, E., and T. Hearn, 1994. Bootstrapping shear-wave splitting errors. Bull. Seismol. Soc. Am., 84 (1994), pp. 1971–1977

Savage, M.K., 1999. Seismic anisotropy and mantle deformation: what have we learned from shear wave splitting? Rev. Geophys. 37, 65–106.

Schneider, D., D.K. Holm, C.O. Boyle, M. Hamilton, and M. Jercinovic, 2004. Paleoproterozoic development of a gneiss dome corridor in the southern Lake Superior region, U.S.A.: In Whitney, Tessyier, and Siddoway (eds) Gneiss domes in orogeny: Geological Society of America Special Paper 380, p.339-357.

Schulz, K.J. and W.F. Cannon, 2007. The Penokean orogeny in the Lake Superior region. Precambrian Research 157: 4.doi:10.1016/j.precamres.2007.02.022.

Silver, P.G., 1996. Seismic Anisotropy Beneath the Continents: Probing the Depths of Geology. Annual Review of Earth and Planetary Sciences, Vol. 24: 385-432, DOI: 10.1146/annurev.earth.24.1.385

Silver, P.G., and W.W. Chan, 1991. Shear-wave splitting and subcontinental mantle deformation, J. Geophys. Res., 96, 16,429–16,454.

Silver, P.G., and S. Kaneshima, 1993. Constraints on mantle anisotropy beneath Precambrian North America from a transportable teleseismic experiment, J. Geophys. Res., 20, 1127– 1130.

Silver, P.G. and M.D. Long, 2011. The non-commutivity of shear wave splitting operators at low frequencies and implications for anisotropy tomography, Geophys. J. Int., 184, 1415–1427.

Sims, P.K., and Z.E. Petermar, 1986. Early Proterozoic Central Plains orogen: A major buried structure in the north-central United States, Geology, 14(6), 488–491

Sol, S., C.J. Thompson, J.M. Kendall, D. White, J.C. VanDecar, and I. Asude, 2002. Seismic tomographic images of the cratonic upper mantle beneath the Western Superior Province of the Canadian Shield–a remnant Archaean slab, Phys. Earth planet. Int., 134, 53–69.

Southwick, D. L., and G. B. Morey, 1991. Tectonic imbrication and foredeep development in the Penokean orogen, east-central Minnesota - an interpretation based on regional geophysics and the results of test-drilling: U.S. Geological Survey bulletin 1904, 17p

Stein, S., et al., 2011. Learning from failure: The SPREE Mid-Continent Rift Experiment, GSA Today, 21(9), 5–7, doi:10.1130/G120A.1.

Stockwell, C.H., J.C. McGlynn, R.F. Emslie, B.V. Sanford, A.W. Norris, J.A. Donaldson, W.F. Fahrig, and K.L. Currie, 1972. Geology of the Canadian shield, in Geology and Economic Minerals of Canada, edited by R.J.W. Douglas, Econ. Geol. Rep. 1, 838 pp., Geol. Surv. of Can., Ottawa.

Stott, G.M., 2011. A revised terrane subdivision of the Superior Province in Ontario; Ontario Geological Survey, Miscellaneous Release—Data 278.

Sutcliffe, R.H., 1991. Proterozoic geology of the Lake Superior area, in Geology of Ontario, Ont. Geol. Surv. Spec. Vol., 4, part 1, 627–658.

Teanby, N.A., J.M. Kendall, M. Van der Baan, 2004. Automation of shear-wave splitting measurements using cluster analysis Bull. Seismol. Soc. Am., 94, pp. 453–463

Thompson, A. B. and J. Ridley, 1987. Pressure-temperature-time (PTt) histories of orogenic belts. In: Tectonic settings of regional metamorphism, (E. R. Oxburgh, B. W. D. Yardley and P. C. England, eds.). Philosophical Transactions of the Royal Society, London, A 321, pp. 27-45.

Tollo, R.P., L. Corriveau, J. McLelland, and M.J. Bartholomew, 2004. Proterozoic tectonic evolution of the Grenville orogen in North America: An introduction. In Tollo, Richard P.; Corriveau, Louise; McLelland, James et al. Proterozoic tectonic evolution of the Grenville orogen in North America. Geological Society of America Memoir 197. :Boulder, CO. pp. 1–18.ISBN 978-0-8137-1197-3.

Tvelia, S. (n.d.). The First Crust and the Development of Continents. [online] This Old Earth. Available at: http://thisoldearth.net/Geology_Online-1_Subchapters.cfm?Chapter=8&Row=2 [Accessed 6 Jul. 2014].

Van der Lee, S., and A. Frederiksen, 2005. Surface wave tomography applied to the North American upper mantle, in Seismic Earth: Array Analysis of Broadband Seismograms, Geophysical Monograph, vol. 157, edited by A. Levander and G. Nolet, pp. 67–80, AGU, Washington D.C.

Van Schmus, R., 1976. Early and Middle Proterozoic history of the Great Lakes area, North America. Royal Society of London Philosophical Transactions, v. 280, p. 605-628.

Van Schmus, W.R., and W. J. Hinze, 1985. The Midcontinent Rift System. Ann. Rev. Earth Planet. Sci. 1985.13: 345—83

Van Schmus, W.R., D.A. Schneider, D.K. Holm, S. Dodson, B.K. Nelson, 2007. New insights into the southern margin of the Archean-Proterozoic transition in the north-central U.S. based on U–Pb, Sm–Nd, and Ar–Ar geochronology. Precambrian Research 157, 80–105

VanArsdale R.B., 2009. Adventures through deep time: the Central Missippi River Valley and its earthquakes. QE78.7.V36 p.cm. – (Special paper; 452) 55.7 – dc22

Vecsey, L., J. Plomerová and V. Babuška, 2008. Shear-wave splitting measurements - Problems and solutions. Tectonophysics, Volume 462, Issues 1–4, 15, Pages 178–196

Vinnik, L., G. Kosarev, and L. Makeyeva, 1984. Anisotropy of the lithosphere according to the observations of SKS and SKKS waves, Dokl. Akad. Nauk SSSR, 278, 1335.

Vinnik L.P., V. Farra, B. Romanowicz, 1989. Azimuthal anisotropy in the earth from observations of SKS at GEOSCOPE and NARS broadband stations, Bull. seism. Soc. Am., 79, 1542–1558.

Walsh, E., 2013. Measuring Shear Wave Splitting using the Silver and Chan Method, Master's dissertation, Victoria University of Wellington, Wellington, New Zealand.

Whitmeyer, S.J., and K.E. Karlstrom, 2007. Tectonic model for the Proterozoic growth of North America, Geosphere, 3, 220–259, doi:10.1130/GES00055.1.

Wolfe, C.J., and P.G. Silver, 1998. Seismic anisotropy of oceanic upper mantle: Shear wave splitting methodologies and observations, J. Geophys. Res., 103, 749– 771.

Wüstefeld, A., and G. Bokelmann, 2007. Null detection in shear-wave splitting measurements. Bull Seism Soc Am 97:1204–1211

Wüstefeld, A., G. Bokelmann, G. Barruol, J. Montagner, 2009. Identifying global seismic anisotropy patterns by correlating shear-wave splitting and surface-wave data. Physics of the Earth and Planetary Interiors 176, 198–212

Wüstefeld, A., G. Bokelmann and G. Barruol, 2010. Evidence for ancient lithospheric deformation in the East European Craton based on mantle seismic anisotropy and crustal magnetics. Tectonophysics, 481, 16-28.

Wynne-Edwards, H.R., 1972. The Grenville Province. In Price, R.A., and Douglas, R.J.W., eds., Variations in tectonic styles in Canada. Geological Association of Canada, Special Paper 11: 263-334

Yardley, G. and S. Crampin, 1991. Extensive-dilatancy anisotropy: relative information in VSPs and reflection surveys, Geophys. Prosp., 39, 337-355.